# STUDIES OF THE MAGNETIC PROPERTIES AND MICROSTRUCTURES OF TWO RARE EARTH-TRANSITION METAL TYPE MAGNETIC ALLOYS

By

Tony Bailey

A thesis submitted for the degree of

Doctor of Philosophy

Department of Metallurgy and Materials,

Faculty of Science and Engineering,

University of Birmingham.

August 1985.

**1st of 3 files**

**Introductory material and chapters 1 to 4**

# The remaining chapters and the appendices are in two additional files

## SYNOPSIS

An investigation into the optimisation of magnetic properties of two types of magnetic alloys based on $Sm(Co,Cu,Fe,Zr)_z$ (z = 7.4) and $Nd_{15}Fe_{77}B_8$ has been carried out.

The optimum heat treatment which gave the best magnetic properties for the $Sm(Co,Cu,Fe,Zr)_z$ alloy depended primarily on the sintering and solid solution temperatures. After quenching the alloy from the solid solution temperature, and then ageing isothermally, it was found that the intrinsic coercivity, microhardness and electrical resistance changed with ageing time, and the ageing temperature also affected the rate of these changes.

The magnetic properties of specimens produced from the Nd-Fe-B type alloy were also shown to be affected by different heat treatments. The microhardness, microstructure and intrinsic coercivity were affected by an isothermal ageing treatment and the temperature of the treatment.

Two routes were used for powder preparation in the production of the sintered specimens:

i. Mechanical ball milling of crushed ingot material.

ii. Hydrogenation followed by ball milling.

It was found that higher energy products were achieved in the ball milled material for the two alloys investigated. Two reasons for this were proposed:

i. The hydrogenated and ball milled powder had a larger size than the ball milled only powder.

ii. The surfaces of the hydrogenated powder were highly reactive in air and some oxidation of the surfaces occurred.

Optical and electron microscope studies showed that the variations in the ageing behaviour of both the alloys was concurrent with subtle differences in the microstructure between the samples aged at different isothermal ageing temperatures.

ACKNOWLEDGEMENTS

The author is very grateful to his supervisor Dr. I.R. Harris for his enthusiastic support, encouragement and useful discussions during the course of this research. Thanks are also extended to Professor R.E. Smallman, Head of Department of Metallurgy and Materials, for the provision of departmental facilities.

The author is grateful to Mr. N.A. Smith for his excellent technical assistance and to Mr. G. Colton for designing parts of the magnetic measuring system. The author would also like to thank all members of the magnet and hydrogen group for many stimulating and useful discussions.

Thanks are due to Rare Earth Products (a Division of Johnson Matthey), for their financial support, the provision of materials and continued interest in this project. Thanks also to Miss C. Green and Miss T. Salliss for typing this thesis.

CONTENTS

# CHAPTER ONE

## GENERAL INTRODUCTION

The rare earth - transition metal (RE - TM) permanent magnets (PMs) have played a conspicuous role in the developments of the electrical and electronic industries and research work with these alloys has been spurred on by these contributions. Attention is always being paid to the production of suitable magnetic material at the lowest possible cost. Before discussing the modern developments in PM technology however, it would be worthwhile to look at the development of PMs since the early fifties.

In the 1950's the advent of barium or strontium ferrites with high coercivity and low remanence (see fig. 1.1 - ref. 1) and much cheaper raw materials cost than the Alnico magnets resulted, over the past 20 years, in a change in the trends in magnet production. In Japan, the ferrites have increased fivefold in production tonnage, while the Alnicos are being produced at less than a third of their 1970 output (see fig. 1.2 - ref. 2) due to the more expensive raw materials used in these alloys (particularly cobalt).

The appearance of rare earth - cobalt magnets around 1960 led to another step forward in terms of improved magnetic properties (see fig. 1.1). The most recent type of rare earth -

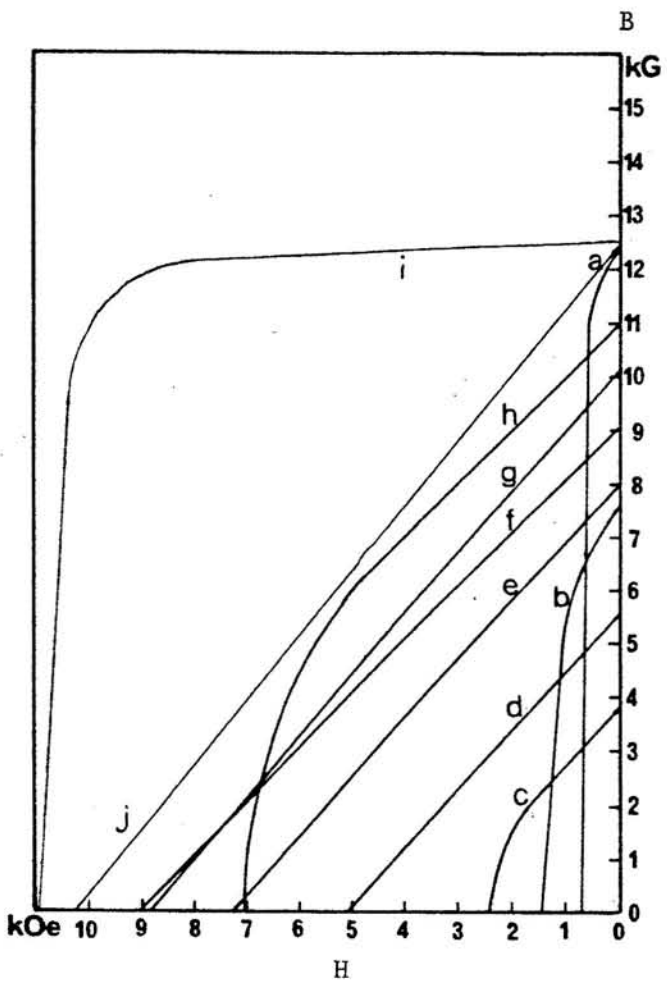


Fig. 1.1 Demagnetization curves of commercial magnets

a,b Alnico type.

c, Ba-Sr, $Fe_3O_4$.

d, $SmCo_5$ (resin bonded)

e, $(MM,Sm)Co_5$.

f, $SmCo_5$ (sintered).

g, $(Sm,Pr)Co_5$.

h, "2:17" type.

i, Nd-Fe-B (Plot of B-H versus H).

j, Nd-Fe-B (Plot of B versus H).

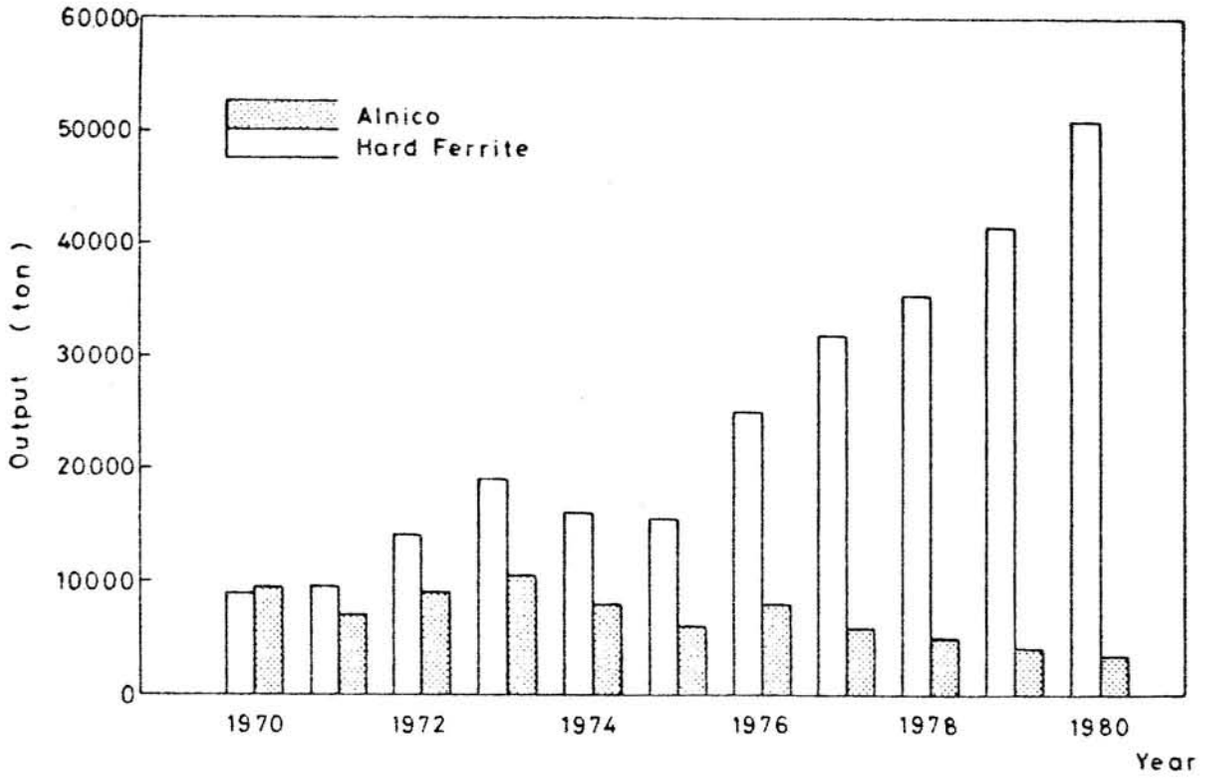


Fig. 1.2 Recent trends of magnet production in Japan.

| | BASTNAESITE | MONAZITE |
|---|---|---|
| $La_2O_3$ | 32 | 23 |
| $Ce_2O_3$ | 49 – 51 | 45 – 47 |
| $Pr_6O_{11}$ | 4 – 5 | 4 – 6 |
| $Nd_2O_3$ | 13 – 16 | 15 – 20 |
| $Sm_2O_3$ | 0.5 – 1 | 3 – 5 |
| Yttric group (10 elements) | ad 100 | ad 100 |

Fig. 1.3 The distribution of rare earths in rare earth ores.

cobalt alloys is the "2:17"-type; commercially available alloys are based on $Sm_2(Co,Cu,Fe,Zr)_{17}$. In 1983, the Sumitomo Company of Japan announced a new development in the field of RE magnet alloys based on a Nd-Fe-B alloy. The material was given the trade name "Neomax" and was reported to have a magnetic force 1.6 times that of the best rare earth - cobalt magnets and energy product of 35 MGOe. The announcement is being followed by much experimental work and despite the Nd-Fe-B alloys having a lower Curie Temperature and poorer oxidation resistance than the "2:17"-type materials, their favourable cost may facilitate their increasing use in many applications now using ferrite and rare earth cobalt magnet materials.

The uses of permanent magnets are numerous; the RE - TM magnets are finding their way into many electrical devices (ref. 3) such as: motors; high fidelity equipment and computer peripheral devices; uses have also been found in medical and dental applications (ref. 4).

## 1.1 Availability of the RE - TM Magnets

The appearance of Nd-Fe-B type alloys as a desirable magnetic alloy affects the RE supply situation. Nd is cheaper due to its greater concentration in RE ores (ref. 5). The attractiveness of this alloy is the large amount of iron present (about 65 weight percent) which significantly decreases the cost over RE - Co alloys.

With regard to the RE - Co - type alloys, cobalt is expensive and supplies have been erratic over the past decade partly because

of unrest in Zaire in 1978, (source of about half the world supply of refined Co metal), and partly because of an unsuccessful attempt by producers to form a cartel. Samarium, is significantly scarcer than Pr and Nd, but new rare earth ore deposits recently discovered particularly in the Bayon Oho mining district of Baotou in Inner Mongolia in conjunction with new rare earth extraction facilities in the U.S. and China have ensured the supply of samarium and the other rare earths. In fig. 1.3 distributions of the RE's are given in the two most common RE ores.

## 1.2 Scope of the Thesis

The electronic structure of the component metals is discussed together with the origins of magnetic behaviour. A review of magnet units, a study of types of magnetism and the theory of magnetic domains is given in some detail. This is followed by a survey of the phase diagrams and crystal structures of the various rare earth alloys.

The experimental work is described stage by stage; the results are presented and discussed together in the penultimate section. Finally a conclusion on the work is made.

## 1.3 The Rare Earth Metals

The "rare earths" are in fact not rare at all; their general lack of availability is due to the difficulty in extracting them from the ore. They are members of Group III-A of the periodic table (see fig. 1.4), with atomic numbers 57 through to 71

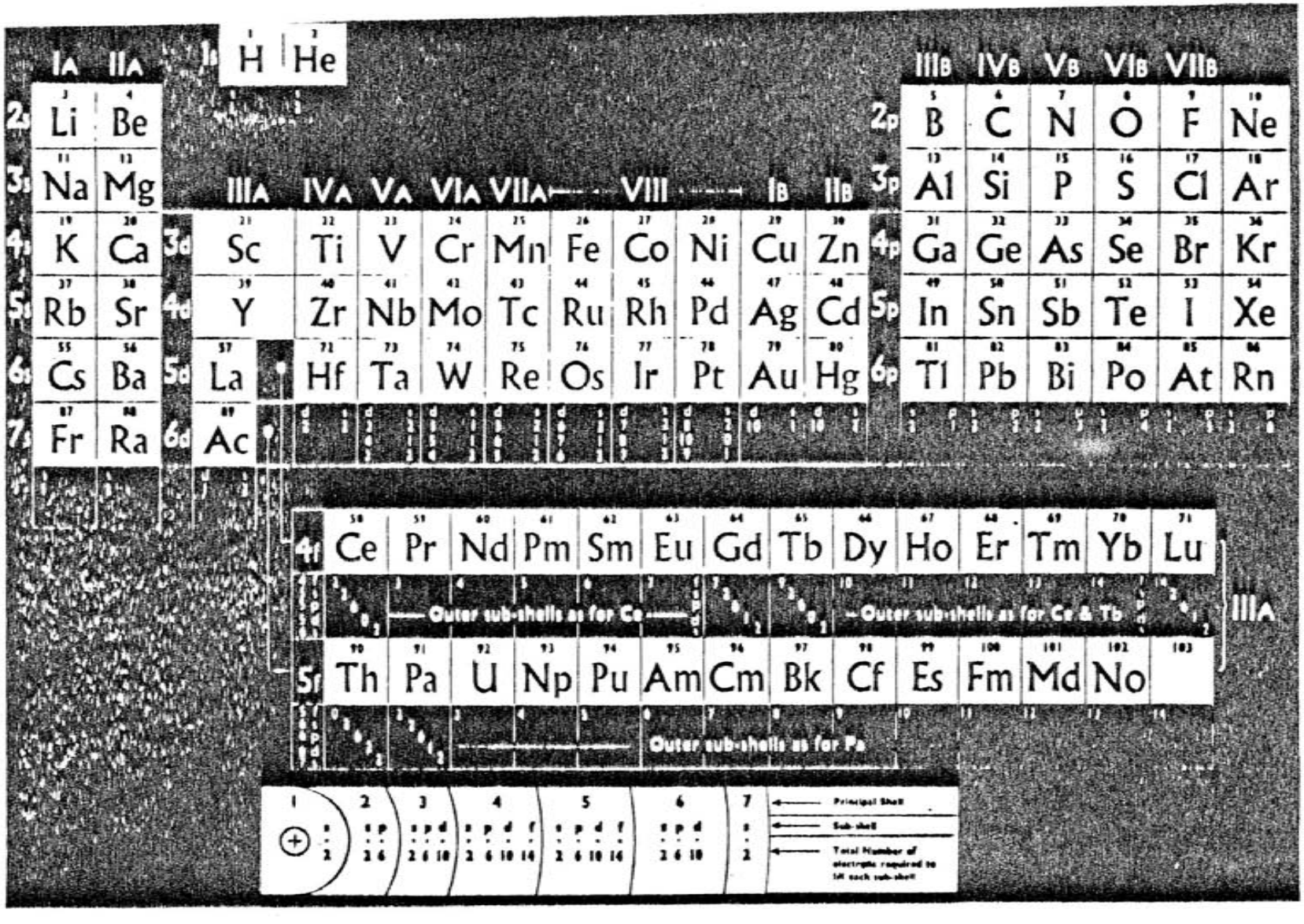


Fig. 1.4 Periodic table.

(lanthanum to lutetium), commonly called the lanthanides.

The electron shells in the 4f state fill up successively with increasing atomic number (see fig. 1.5). The rare earths have a very similar outer valence electron configuration, resulting in close chemical and physical properties. Because the 4f electrons are so deep in the atom, they are shielded from the crystalline electric field of the surrounding ions; the orbital moment is therefore not quenched and the total magnetic moment has both orbital and spin components.

## 1.4 The Lanthanide Contraction

The lanthanide contraction consists of a decrease in atom size with increasing atomic number; this is important in determining the rare earth magnetic and other properties. It is brought about by the fact that the shielding of one 4f electron by another is imperfect due to the shapes of the orbitals. Thus at each atomic number increment the effective nuclear charge experienced by each 4f electron increases, thus causing a reduction in size of the entire $4f^n$ shell.

## 1.5 The Transition Series

These occur in the periodic table with partially filled 3d, 4d and 5d shells (see fig. 1.5). Since these orbitals tend to project out to the atom periphery the orbital motions are affected by crystal fields, and therefore by the environment where they are found - the orbitals are said to be "quenched". Therefore the magnetic moment is due to electron spin, which is

| Atomic No. and symbol | | State $n$ $l$ | 1s 1 0 | 2s 2 0 | 2p 2 1 | 3s 3 0 | 3p 3 1 | 3d 3 2 | 4s 4 0 | 4p 4 1 | 4d 4 2 | 4f 4 3 | 5s 5 0 | 5p 5 1 | 5d 5 2 | 6s 6 0 |
|---|---|---|---|---|---|---|---|---|---|---|---|---|---|---|---|---|
| 18 | Ar | | 2 | 2 | 6 | 2 | 6 | | | | | | | | | |
| 19 | K | | 2 | 2 | 6 | 2 | 6 | – | 1 | | | | | | | |
| 20 | Ca | | 2 | 2 | 6 | 2 | 6 | – | 2 | | | | | | | |
| 21 | Sc | | 2 | 2 | 6 | 2 | 6 | 1 | 2 | | | | | | | |
| 22 | Ti | | 2 | 2 | 6 | 2 | 6 | 2 | 2 | | | | | | | |
| 23 | V | | 2 | 2 | 6 | 2 | 6 | 3 | 2 | | | | | | | |
| 24 | Cr | | 2 | 2 | 6 | 2 | 6 | 5 | 1 | | | | | | | |
| 25 | Mn | | 2 | 2 | 6 | 2 | 6 | 5 | 1 | | | | | | | |
| 26 | Fe | | 2 | 2 | 6 | 2 | 6 | 6 | 2 | | | | | | | |
| 27 | Co | | 2 | 2 | 6 | 2 | 6 | 7 | 2 | | | | | | | |
| 28 | Ni | | 2 | 2 | 6 | 2 | 6 | 8 | 2 | | | | | | | |
| 29 | Cu | | 2 | 2 | 6 | 2 | 6 | 10 | 1 | | | | | | | |
| 54 | Xe | | 2 | 2 | 6 | 2 | 6 | 10 | 2 | 6 | 10 | – | 2 | 6 | | |
| 55 | Cs | | 2 | 2 | 6 | 2 | 6 | 10 | 2 | 6 | 10 | – | 2 | 6 | | 1 |
| 56 | Ba | | 2 | 2 | 6 | 2 | 6 | 10 | 2 | 6 | 10 | – | 2 | 6 | | 2 |
| 57 | La | | 2 | 2 | 6 | 2 | 6 | 10 | 2 | 6 | 10 | – | 2 | 6 | 1 | 2 |
| 58 | Ce | | 2 | 2 | 6 | 2 | 6 | 10 | 2 | 6 | 10 | 1 | 2 | 6 | 1 | 2 |
| 59 | Pr | | 2 | 2 | 6 | 2 | 6 | 10 | 2 | 6 | 10 | 2 | 2 | 6 | 1 | 2 |
| 60 | Nd | | 2 | 2 | 6 | 2 | 6 | 10 | 2 | 6 | 10 | 3 | 2 | 6 | 1 | 2 |
| 61 | Pm | | 2 | 2 | 6 | 2 | 5 | 10 | 2 | 6 | 10 | 4 | 2 | 6 | 1 | 2 |
| 62 | Sm | | 2 | 2 | 6 | 2 | 6 | 10 | 2 | 6 | 10 | 5/6 | 2 | 6 | 0/1 | 2 |
| 63 | Eu | | 2 | 2 | 6 | 2 | 6 | 10 | 2 | 6 | 10 | 7 | 2 | 6 | | 2 |
| 64 | Fs | | 2 | 2 | 6 | 2 | 6 | 10 | 2 | 6 | 10 | 7 | 2 | 6 | 1 | 2 |
| 65 | Tb | | 2 | 2 | 6 | 2 | 6 | 10 | 2 | 6 | 10 | 8 | 2 | 6 | 1 | 2 |
| 66 | Dy | | 2 | 2 | 6 | 2 | 6 | 10 | 2 | 6 | 10 | 9 | 2 | 6 | 1 | 2 |
| 67 | Ho | | 2 | 2 | 6 | 2 | 6 | 10 | 2 | 6 | 10 | 10 | 2 | 6 | 1 | 2 |
| 68 | Er | | 2 | 2 | 6 | 2 | 6 | 10 | 2 | 6 | 10 | 11 | 2 | 6 | 1 | 2 |
| 69 | Tm | | 2 | 2 | 6 | 2 | 6 | 10 | 2 | 6 | 10 | 12/13 | 2 | 6 | 0/1 | 2 |
| 70 | Yb | | 2 | 2 | 6 | 2 | 6 | 10 | 2 | 6 | 10 | 14 | 2 | 6 | | 2 |
| 71 | Lu | | 2 | 2 | 6 | 2 | 6 | 10 | 2 | 6 | 10 | 14 | 2 | 6 | 1 | 2 |
| 72 | Hf | | 2 | 2 | 6 | 2 | 6 | 10 | 2 | 6 | 10 | 14 | 2 | 6 | 2 | 2 |

Fig. 1.5 Electron states in transition metals and rare earths.

important particularly in the ferromagnetic 3d metals including Fe, Co and Ni as alloying with other components can have a marked effect on the magnetic behaviour.

## 1.6 Magnetism in the Rare Earth - Transition Metal Alloys

Several of the rare earth elements display magnetic ordering and large magnetic moments at low temperatures. Secondly, due to the large difference in atomic radii between the RE and Mn, Fe, Co and Ni atoms there is a tendency to form several intermetallic compounds in the binary system with a hexagonal structure. Thirdly, many of these intermetallic compounds exhibit magnetic ordering by the coupling of the rare earth magnetic moment with the 3d transition element moment.

In the 3d magnetic elements Fe, Co and Ni large 3d exchange interactions stabilize ferromagnetic ordering well above room temperature, but because the orbital moments are "quenched" the magnetic anisotropy is generally very small, thus limiting the coercivity of the 3d elements. The rare earths on the contrary exhibit large orbital moments, but the 4f magnetic interactions are much smaller than those of the 3d electrons and the ordered magnetic state is attained only below room temperature. In RE - TM alloys however, 4f and 3d electron interactions can occur, so that, the 3d interactions stabilize the magnetic ordering to above room temperature and the 4f anisotropy remains strong at room temperature.

Thus, a convenient combining of the magnetic and crystal characteristics can occur in some RE - TM alloys giving rise to significant improvements in the magnetic properties.

# CHAPTER TWO

# THEORIES OF MAGNETISM

## 2.1 Units of Magnetism

In the field of magnetism most scientific workers have used the cgs system of measurement. The SI system has been used increasingly since about 1983. The results reported in this thesis are presented in the cgs system in line with the vast amount of existing information. However, as a comparison the conversions and relationships of the two systems are given in table 2.1.

## 2.2 Definitions of Magnetic Quantities

A detailed study of the various magnetic quantities used in the area of magnetism can be found in most standard texts on magnetism (see for example refs. 7,8,9). A summary of the definitions of magnetic quantities is given in table 2.2.

### 2.2.1 Magnetization Curves and Hysteresis Loops

A discussion of the effects of applied fields on materials is useful at this point as it will aid in defining magnetic quantities used later in the work.

#### 2.2.1 I Remanence and Coercivity

If a permanent magnetic material is placed between the poles

Table 2.1

Units of Magnetic Quantities

| Quantity | cgs unit (emu) | SI unit | Relations between the units |
|---|---|---|---|
| Permeability of free space | Unity | $\mu_o = 4\pi \times 10^{-7}$ weber $A^{-1}m^{-1}$ | |
| Induction in free space (field) | B Gauss (G) | $B_o$ Tesla (T) | $1G = 10^{-4}$ T |
| Magnetic field | H Oersted (Oe) | H ($Am^{-1}$) | $1Oe = 79.58\ Am^{-1}$ |
| Induction in free space | B = H | $B_o = \mu_o H$ | $1Oe = 10^{-4}$ T |
| Induction in medium | B = H + 4 M | $B = B_o + \mu_o M = \mu_o (H + M)$ | $1G = 10^{-4}$ T |
| Magnetization per unit volume | M($ergOe^{-1}cm^{-3}$) ($emucm^{-3}$) | M ($JT^{-1}M^{-3}$) | $1\ emucm^{-3} = 10^{3}\ JT^{-1}m^{-3}$ |
| Magnetization per unit mass | $\sigma = M/\rho$ ($erg\ Oe^{-1}g^{-1}$) | $\sigma = \frac{M}{\rho}$ ($JT^{-1}\ kg^{-1}$) | $1\ ergOe^{-1}g^{-1} = 1\ JT^{-1}\ kg^{-1}$ |
| Susceptibility per unit volume | $K = M/H$ ($ergOe^{-2}cm^{-3}$) | $K = \frac{M}{B_o}$ ($JT^{-2}M^{-3}$) | $1\ ergOe^{-2}cm^{-3} = 10^{7}\ JT^{-2}m^{-3}$ |
| Susceptibility per unit mass | $x = K/\rho$ ($ergOe^{-2}g^{-1}$) | $x = K/\rho$ ($JT^{-2}kg^{-1}$) | $1\ ergOe^{-2}g^{-1} = 10^{4}\ JT^{-2}kg^{-1}$ |
| Bohr magneton | $\mu_B = eh/4\pi mc$ $= 9.2732 \times 10^{-21}\ ergOe^{-1}$ | $\mu_B = eh/4\pi mc$ $= 9.2732 \times 10^{-24}\ JT^{-1}$ | |
| Maximum energy product | $BH_{max}$ (MGOe) | $BH_{max}$ ($kJm^{-3}$) | $1\ MGOe = 7.958\ kJm^{-3}$ |

table 2.2 Definitions of Magnetic Quantities

| Magnetic Quality | Symbol | Definition |
|---|---|---|
| Unit Pole | P | The field created by a unit pole has an intensity of one Oe at a distance of 1 cm from the pole. |
| Magnetic field | H | A field of unit strength (ie. 1 Oe) exerts a force of one dyne on a unit pole. |
| Magnetic moment | m | $m = PlH\sin\theta$. P is the pole strength at the ends of a magnet of length l and at an angle $\theta$ in a uniform field H. |
| Magnetization | M | The intensity of magnetization or magnetization is the pole strength per unit cross sectional area, $(= \frac{P}{a})$. |
| Specific magnetization | $\sigma$ | The magnetization per unit mass |
| Magnetizing flux | $\phi$ | The number of lines of force (measured in Maxwells) cutting a given area at right angles. |
| Magnetic Induction | B | This is the flux per unit area at right angles to the flux direction. It is the vector sum of the magnetization and the magnetic field (ie. $B = H + 4\pi M$). |
| Magnetic susceptibility | K | $K = \frac{M}{H}$ |
| Magnetic permeability | $\mu$ | $\mu = \frac{B}{H}$ |
| Bohr Magneton | $\mu_B$ | $\mu_B = \frac{eh}{4\pi mc}$ e = electron change<br>h = Planck's constant<br>m = electron mass<br>c = speed of light |

of an electromagnet then a plot of B, (the magnetic induction) versus H, (increasing applied field), will show a curve OPQ as in fig. 2.1. If H is reduced to zero, B still has a positive value $B_r$ and it is necessary to apply a negative magnetizing force $H_c$ to reduce B to zero. If H is reversed several times between the same positive and negative limits a symmetrical loop $QB_rH_cQ'B_rH_c'Q$ results; this is called a hysteresis loop. When H reaches a value sufficient to saturate the magnetic material, the area of the loop ceases to grow.

The second quadrant of the hysteresis loop with B positive and H negative is important in describing the quality of a permanent magnetic material. There is one point between $B_r$ and $H_c$ for which the product of B and H has a maximum value, this is called the maximum energy product $BH_{max}$. The magnetic induction B also includes contributions from the external field of the electromagnet; thus B is not a measure of the state of a permanent magnet material. It is usual to plot the magnetization B-H (= $4\pi M$) against field together with a B against H plot. As shown in fig. 2.2 the value of H for which B-H is zero is called $_iH_c$, the intrinsic coercivity and $_bH_c$ (induction coercivity) when B is zero. $B_r$ is the remanence.

### 2.2.1 II Squareness Factors

Squareness factors are useful in determining the stability of a permanent magnet while undergoing demagnetization. Looking at the B-H versus H plot in fig. 2.3, $H_k$ is the value of the applied field corresponding to 90% of the remanence Br.

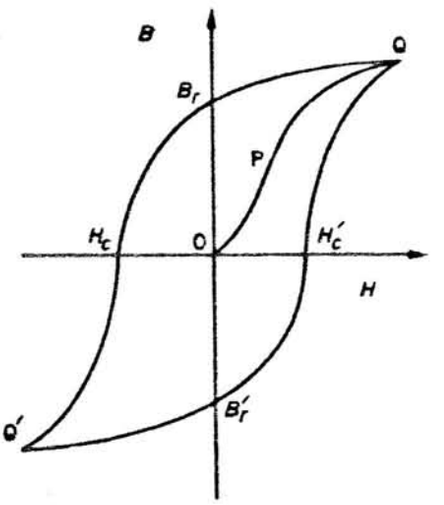


Fig. 2.1 Initial magnetization and hysteresis loop.

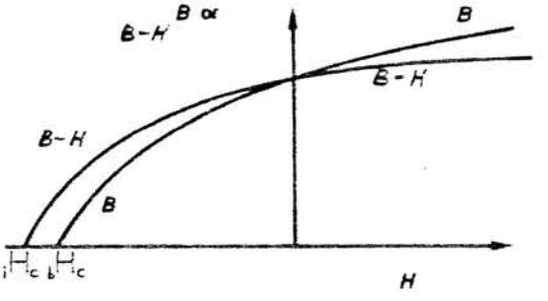


Fig. 2.2 B and B-H versus H.

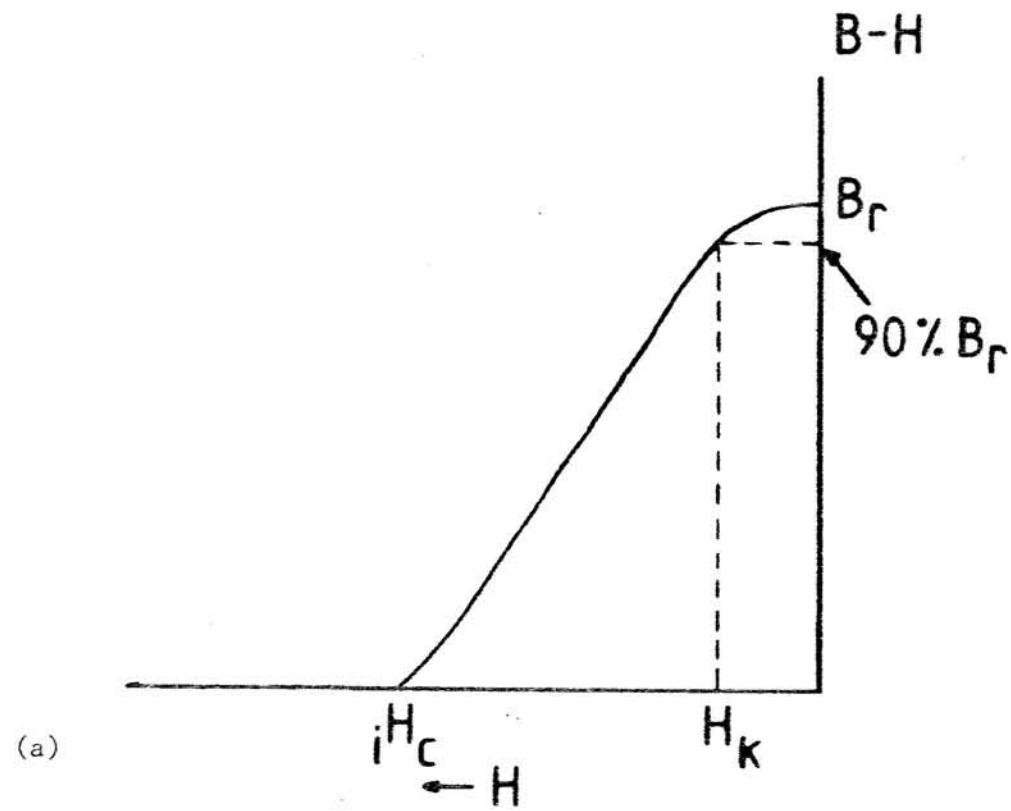


(a)

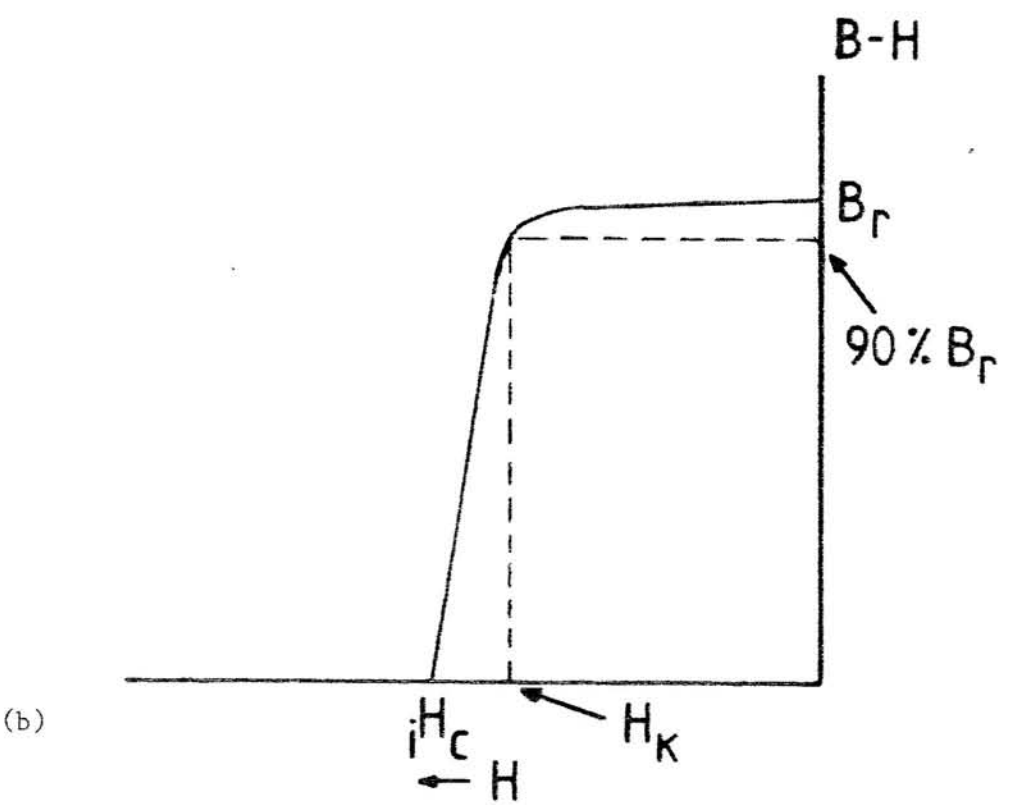


(b)

Fig. 2.3 Two types of B-H versus H plots showing the range of possible squareness factor values: a) $H_K/_{iH_c} \to 0$.
b) $H_K/_{iH_c} \to 1$.

Therefore the squareness can be defined as:

$$\text{Squareness factor} = \frac{H_k}{{}_iH_c} \qquad (2.1)$$

$H_k$ will approximate to ${}_iH_c$ for an almost perfect square curve (as indicated in fig. 2.3) and the factor will tend to 1. For a less square curve, the factor decreases towards zero.

For many magnetic applications it is required that the magnet maintains all its induction when exposed to potential demagnetizing fields so a squareness close to 1 would be desirable. Some magnets might merely need a high $B_r$ or ${}_iH_c$ or both and the squareness would be less important. The various properties required for various applications are itemised in table 2.3.

## 2.3 Types of Magnetism

A description of the types of magnetic behaviour is given below; more detailed reviews appear in a number of standard texts (see for example refs. 7,8,9).

### 2.3.1 Diamagnetism

Diamagnetic substances exhibit a negative response to a magnetic field and a susceptibility less than zero. All substances have a basic diamagnetic term but it is nearly always weak and very often masked by a much larger paramagnetic term. The diamagnetic effect is caused by the influence of an applied field on the motion of electrons. This is illustrated by considering an unmagnetized material where the planes of the orbits are oriented at random.

Table 2.3

Various magnetic property requirements for different applications.

| Applications | Important magnetic properties | Additional data needs | Special concerns |
|---|---|---|---|
| **Microwave tubes:** Traveling Wave Tubes, Klystrons, etc. | Coercive Force, Energy Product, Reversible & Irreversible Loss | Reversible & Irreversible Loss data for various loadlines, Demagnet. curves as a function of temp. -100 to 300°C, External field effects (1 ~ 8 kOe). | Reduce Irreversible Loss, Variations in property values from one lot to another and within a given lot |
| **Rotating machinery:** | High Remanence, High Coercivity, Slope of B-H curve | Long Term Stability data at elevated temp., Recoil Permeability as a function of temperature | Would like to see higher Induction values, Variation in properties for larger magnets |
| **Magnetic bearings:** | All Properties, Intrinsic Coercive Force | Long Term Stability data at normal & elevated temperature | Homogeneity, Uniformly magnetized radial magnets |
| **Precision aerospace instruments:** | All Properties | Long Term Stability data at normal & elevated temperature | Will trade properties for physical strength |

The introduction of an applied field causes these orbits to precess about the field. The precession produces a small field in opposition to the applied field (analogous to Lenz's law of electromagnetic induction) and a negative susceptibility results.

### 2.3.2 Paramagnetism

Paramagnetic substances exhibit a temperature dependent slightly positive susceptibility in an applied field.

#### 2.3.2 I Classical Theory

In 1905 Langevin considered paramagnetism in terms of a paramagnetic gas in which each particle was endowed with a permanent magnetic moment, so that when a mass of the gas was placed in a field each particle tended to set with its magnetic axis parallel to it. The particles are prevented from taking up exact alignment in the field because of thermal agitation, but a statistical equilibrium is set up with a majority of the particles contributing to a magnetization parallel to the field.

The molar susceptibility of a paramagnetic substance varies inversely as the absolute temperature, a statement which is known as the Curie Law. On the whole, however, paramagnetic susceptibilities follow a modified Curie Law known as the Curie-Weiss Law where:

$$\chi_m = \text{molar susceptibility} = \frac{C}{T - \theta} \qquad (2.2)$$

$\theta$ is a constant with the dimensions of temperature, for any

one substance. $\theta$ is zero for materials that obey the Curie Law where $\chi_m = \frac{C}{T}$ .

2.3.2 II Quantum Theory of Paramagnetism

In the quantum theory the angle between the magnetic moment and applied field cannot have any value, as assumed in the Langevin theory, but only certain discrete values determined by quantum conditions. The interactions between the various atomic or molecular moments also modify the theory. The classical theory is merely modified by the quantum theory, which improves the quantitative agreement between theory and experiment. The restriction on the angles between moments and fields is given the name "space quantization"; it is illustrated in fig. 2.4. A further study of the quantum theory of paramagnetism may be found in ref. 7.

2.3.3 Ferromagnetism

In ferromagnetic materials a magnetic moment exists even in the absence of any magnetic field and the magnetization is said to be spontaneous. The atomic dipole moments are strongly aligned and parallel. Ferromagnetic elements include Fe, Ni, Co and Gd and their alloys with one another, and also some alloys not containing any of these ferromagnetic materials.

Above the Curie Temperature $T_c$, the spontaneous magnetization disappears and the material becomes paramagnetic following the Curie-Weiss Law (see equation 2.2) with a value of $\theta$ approximately equal to $T_c$.

Weiss explained ferromagnetism by postulating the existence of a "molecular field" which, below $T_c$ was very large, so large in fact that a spontaneous magnetization could occur which magnetized the material to saturation even in the absence of an applied field. Furthermore, Weiss suggested why a ferromagnetic material can be found in the non-magnetic state; by introducing the idea that, in a ferromagnetic material, regions existed called "domains" that were each spontaneously magnetized to the saturation value $M_s$. If the directions of the magnetic moments of each domain are oriented randomly then the overall moment will be zero.

Heisenberg suggested that the Weiss molecular field might be accounted for by an exchange interaction between spinning electrons in particular orbits. Heisenberg further stated that the associated exchange energy between two atoms is a function of the ratio of atomic separation to the diameter of the unfilled shell. The exchange energy is zero at large atomic separations, increases rapidly and causes parallel coupling as the separation diminishes, passing through a maximum, and then decreasing. At a still closer spacing, the exchange energy becomes negative. In this situation, there is antiparallel coupling of the unfilled shells giving rise to antiferromagnetism. The ratio of the atomic spacing to the unfilled shell diameter is largest for iron, nickel and cobalt, the ratio is not sufficiently large for manganese which is antiferromagnetic, this is shown theoretically in fig. 2.5.

The magnetic moment caused by the spinning electron is directed parallel to the field or antiparallel to it. Where there

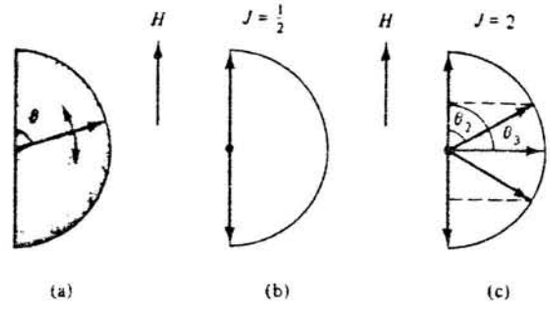


Fig. 2.4 Space quantization a: classical case,
b and c: two quantum possibilities.
(J = S + L).

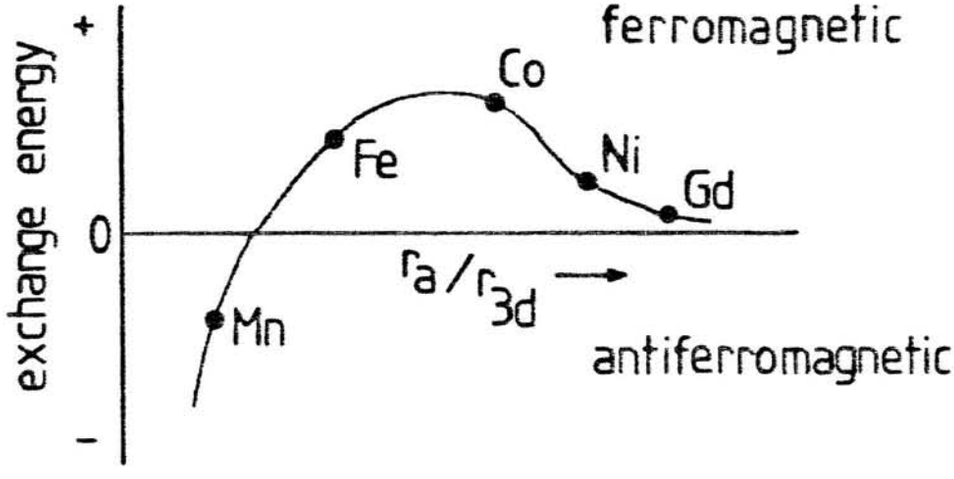


Fig. 2.5 Hypothetical Bethe-Slater curve showing the sign of the exchange energy as a function of the ratio of the atom radius to the 3d electron shell radius.

are two oppositely directed electrons in a shell, their moments cancel and only a small diamagnetic magnetic moment in one direction can arise. The origin of ferromagnetism however is explained on the basis of an electron spin imbalance. For example Fe, Ni and Co contain partly filled 3d shells. The 3d band can accommodate 10 electrons per atom: 5 with plus spins (+ 3d) and 5 with minus spins (- 3d). In the presence of an internal magnetic field as many as possible of the electrons have plus spins; the remainder, minus. In iron, with eight electrons distributed in the 4s and 3d shells, a distribution is calculated to give 0.6 electrons in the 4s, and 4.8 in the + 3d and 2.6 in the - 3d. The resulting spin balance is 2.2 $\mu_B$. It is this unpairing that is responsible for the large magnetic moment in iron and also occurs to a lesser extent in the other 3d elements as shown in table 2.4. The overlapping of the 4s and 3d electron shells also explains why the observed and calculated saturation magnetizations are different as shown in table 2.5. The general rule is that:

$$\text{magnetic moment/atom} = (10.6 - n)\mu_B \qquad (2.3)$$

where n is the total number of 4s and 3d electrons and

$\mu_B$ is the Bohr magneton, and assuming that Ni has 0.6 electrons per atom.

The criteria for ferromagnetism in a metal can be summarized, now that the exchange interaction and band (unpaired electron) theory have been discussed. They place further limitations on which materials can be ferromagnetic:

table 2.4 Spin imbalance as a consequence of the disposition of electrons in the 3d and 4s shells

| Element | Total electrons in the 3d and 4s shells | Electrons in: | | | Unpaired electrons in 3d shell |
|---|---|---|---|---|---|
| | | 4s | +3d | -3d | |
| Cr | 6 | .6 | 2.7 | 2.7 | 0 |
| Mn | 7 | .6 | 3.2 | 3.2 | 0 |
| Fe | 8 | .6 | 4.8 | 2.6 | 2.2 |
| Co | 9 | .7 | 5 | 3.3 | 1.7 |
| Ni | 10 | .6 | 5 | 4.4 | 0.6 |
| Cu | 11 | 1.0 | 5 | 5 | 0 |

table 2.5 Observed and calculated magnetic moments

| | Mn | Fe | Co | Ni |
|---|---|---|---|---|
| total number of 4s and 3d electrons | 7 | 8 | 9 | 10 |
| magnetic moment (observed) ($^{\mu B}/_{atom}$) | 0 | 2.2 | 1.7 | 0.6 |
| magnetic moment (calculated) ($^{\mu B}/_{atom}$) | 3.6 | 2.6 | 1.6 | 0.6 |

1. The electrons responsible for ferromagnetism must lie in partially filled bands so that unpaired electrons have closely spaced, vacant energy levels to move into.

2. The density of levels in the band must be high, so that the increase in energy caused by spin alignment is small.

3. The atoms must be the correct distance apart so that the exchange force can align the relevant electron spins.

### 2.3.4 Antiferromagnetism

The theory of antiferromagnetism was developed mainly by Néel, in which he applied Weiss' Molecular Field Theory to the problem. In an antiferromagnetic material the moments in alternate atoms are ordered in an antiparallel manner. The magnetic behaviour of antiferromagnetic materials differs slightly from that of paramagnetic materials. At a temperature analogous to the Curie temperature of ferromagnetic materials, called the Néel point, the antiferromagnetism disappears and the material behaves like a paramagnet. Antiferromagnetic materials are mainly ionic components, namely oxides, sulphides and chlorides, they are of scientific but not commercial interest, due to their poor magnetic properties.

### 2.3.5 Ferrimagnetism

In a ferrimagnetic material, atomic moments are ordered in an antiparallel sense, but the sum of the moments pointing in one direction exceeds that of those pointing in the opposite direction

so that there is a net magnetic moment. Fig. 2.6 illustrates simply the difference between ferromagnetic, antiferromagnetic and ferrimagnetic ordering. Ferrimagnets are similar to ferromagnets in that they consist of self saturated domains, and exhibit magnetic saturation and hysteresis. Additionally, as in the case of ferromagnets, ferrimagnets become paramagnetic above a Curie temperature.

The most important ferrimagnetic substances are the ferrites, consisting of certain double oxides of iron and another metal. The ferrites fall into two groups with different crystal structure: a cubic structure and the hexagonal structure consisting of the commercially important barium ferrite $BaO.6Fe_2O_3$ and strontium ferrite $SrO.6Fe_2O_3$ which are both magnetically hard. In fig. 2.7 a graphical summary is shown of the temperature effects on the various types of magnetism.

## 2.4 Magnetic Anisotropy

### 2.4.1 Magnetocrystalline Anisotropy

A ferromagnetic single crystal can be magnetized to saturation more easily in certain directions than others. This gives rise to an easy axis of magnetization, and determines the potential energy of the crystal as it is lowest when the material is magnetized in an easy direction. This is illustrated in fig. 2.8 (a,b); when a field is applied to a single crystal in different directions, curves such as those shown can result. The curves show that b.c.c. Fe has an easy axis in the direction [100] while Co has an easy direction along the c-axis [0001] in the hexagonal crystal.

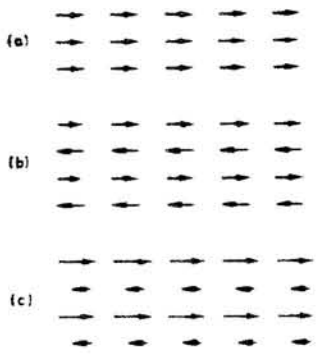


Fig. 2.6 Types of magnetic ordering a) ferromagnetic, b) antiferromagnetic, c) ferrimagnetic.

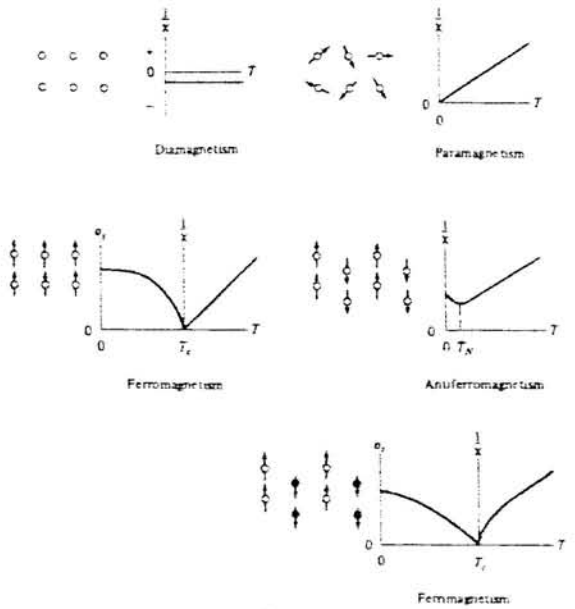


Fig. 2.7 Effects of temperature on various types of magnetic behaviour.

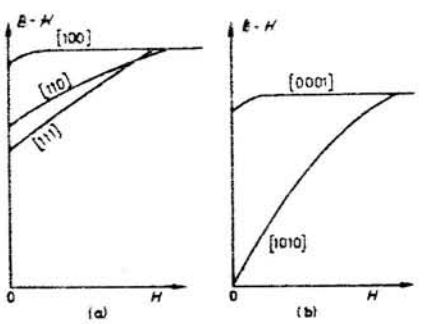


Fig. 2.8 Approximate magnetization in various crystal directions.

To magnetize a single crystal in a hard direction requires an additional energy $E_K$, called the magnetocrystalline anisotropy energy, stored in the crystal magnetized along the hard direction. For a material with uniaxial anisotropy such as hexagonal Co, the anisotropy energy is given by:

$$E_K = K + K_1 \sin^2 \theta + K_2 \sin^4 \theta + \ldots \tag{2.4}$$

$\theta$ is the angle between the direction of magnetization and the single uniaxial easy direction. $K_1$ and $K_2$ are constants which vary with temperature and differ for different materials.

In a cubic material the variation of anisotropy energy with the three cubic axes can be defined as:

$$E_K = K_o + K_1(\alpha_1^2\alpha_2^2 + \alpha_2^2\alpha_3^2 + \alpha_3^2\alpha_1^2) + K_2(\alpha_1^2\alpha_2^2\alpha_3^2) \tag{2.5}$$

$\alpha_1$, $\alpha_2$, $\alpha_3$ are the direction cosines of magnetization direction with respect to the cubic axes of the crystal. In cubic materials, the easy directions are along the cube edges if $K_1$ is positive and $K_2$ is not less than $-\frac{9}{4} K_1$. If $K_1$ is negative, the easy directions lie along the cube diagonals.

Crystal anisotropy is due to spin-orbit coupling. When an external field is applied to a ferromagnet, it tries to re-orientate the electron spin, and the orbital motion tries to change also. But the orbit is strongly coupled to the lattice and can resist the attempt to rotate the spin axis. The energy required to rotate the spin system of an aligned region (that is a domain)

away from the easy direction is called the anisotropy energy and is the energy required to overcome spin-orbit coupling.

### 2.4.2 Shape Anisotropy

Any magnetic body with an elongated shape possesses anisotropy in the sense that, if free to rotate, it aligns with its greatest length parallel to an external field, a larger field is required to magnetize it to saturation parallel to a short dimension because the demagnetizing field is larger. Therefore shape can be a source of magnetic anistropy. The energy associated with shape anisotropy is a magnetostatic energy $E_{ms}$, expressed as:

$$E_{ms} = K_s \sin^2 \theta \tag{2.6}$$

$K_s$ is a shape anisotropy constant and $\theta$ is the angle between the magnetization and easy axis direction.

### 2.4.3 Stress Anisotropy

If the magnetization curve of Ni is measured while under tension, a change takes place in the loop shape as shown in fig. 2.9. The difference is due to magnetostriction; when Ni is magnetized it contracts in the direction of magnetization and expands in the transverse direction. Therefore a stress anisotropy can occur and has an energy associated with it called the magnetoelastic energy $E_{me}$, expressed as:

$$E_{me} = K_\sigma \sin^2 \theta \tag{2.7}$$

$K_\sigma$ is the stress anisotropy constant and $\theta$ is the angle between the magnetization and easy axis directions.

## 2.5 Magnetic Domains

A magnetic material consists of regions where the electron spins are aligned parallel; in the unmagnetized state the spins from each region or domain are pointing randomly and so there is no net magnetic moment. The process of magnetization and the magnetic properties of a material are dependent on the behaviour of the domains. Domains may be defined as regions in which the spontaneous magnetization has the same direction.

Weiss in 1906 originally postulated the existence of domains to explain why a piece of iron could exist in an unmagnetized state. It was not until 40 years later that any application of the domain idea was made to explain the shape of the magnetization curve or magnetic hysteresis.

The origin of domains can be illustrated by considering a large single crystal spontaneously magnetized parallel to the easy axis, as in fig. 2.10a. The free poles at the ends are the source of a field with a consequent magnetostatic energy. This energy can be halved if the crystal splits up into two domains magnetized in opposite directions as in fig. 2.10b. This process will continue as in fig. 2.10c until a domain size is reached where the domain wall energy produced by the splitting of domains is balanced by the magnetostatic energy.

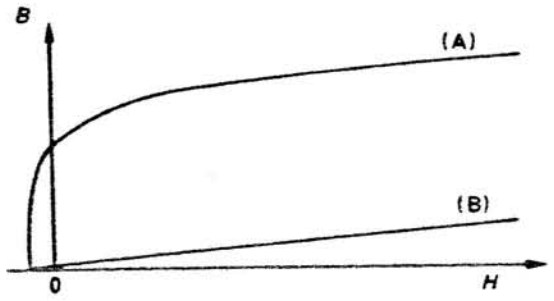


Fig. 2.9 Influence of magnetostriction on magnetic induction.
a) No tension, b) 33 kg $mm^{-2}$.

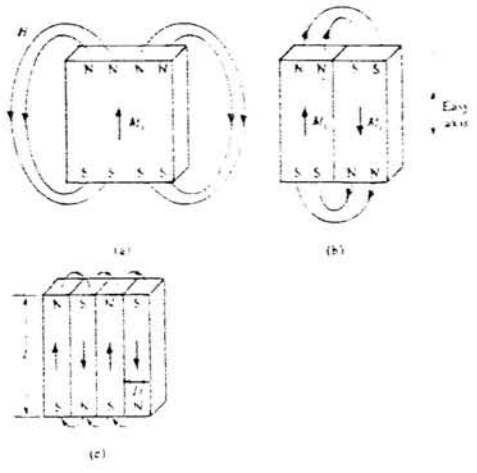

Fig. 2.10 Division into domains.

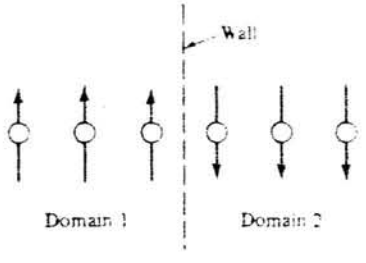


Fig. 2.11 Hypothetical infinitely thin domain wall.

### 2.5.1 Experimental Evidence for Domains

There are several experimental methods for revealing the existence of domains; one of the first used was the powder pattern method developed by Bitter (see ref. 7). This method consists of preparing a colloidal solution of a magnetic powder in a low viscosity liquid; a drop of the solution is placed on the specimen surface which has been carefully polished to avoid any surface stresses which might distort the patterns. The patterns are then observed using an optical microscope. Other methods are based on magneto-optical effects where domains are distinguished from one another by a difference in contrast. The Kerr effect (ref. 7) involves a rotation of the plane of polarization of a beam of light during reflection fom a magnetized specimen, the rotation is dependent on the degree and direction of domain magnetization. The Faraday method (ref. 7) is similar to the Kerr effect but consists of a rotation of the plane of polarization of a light beam as it is transmitted through a specimen. The advantage of this method is that a high contrast is obtainable. Both these methods enable the use of dynamic domain studies.

### 2.5.2 Domain Theory

The interfaces between domains are called domain or Bloch walls; Bloch made the first theoretical examination of the domain wall structure in 1932. At or within the domain wall the magnetization must change direction. The change, rather than being an abrupt one as shown in fig. 2.11, consists of a gradual

change of spin direction thus minimising the exchange energy by avoiding neighbouring spins being antiparallel; this configuration is shown in fig. 2.12. Domain walls can be of the $180^{o}$ or $90^{o}$ type depending on the easy axis of magnetization; iron whose easy axes are at $90^{o}$ to each other can have $90^{o}$ domains where the structure consists of a spin rotation of only $90^{o}$; in some rare earth - transition metal alloys the easy axis is in the c-direction, so only $180^{o}$ domains will occur. A domain wall has a finite width and certain structure. If the angle between adjacent spins is small then the exchange energy is small. However, the crystal anisotropy energy is high if there are a large number of spins pointing in non-easy directions. Therefore there is a compromise situation: while the exchange energy tries to make the wall as wide as possible, the anisotropy energy tries to make the wall thin, in order to reduce the number of spins pointing in non-easy directions; this determines the wall thickness. This is illustrated in fig. 2.13 where the total wall energy $\gamma$ reaches a minimum for a certain wall thickness, $\gamma_{an}$ and $\gamma_{ex}$ are the anisotropy and exchange energies respectively and $\gamma$ is a minimum when these two are equal.

### 2.5.3 Changes in Domain Structure

The process of magnetization involves replacing a multidomain sample with a single domain. This is illustrated in the case of a crystal of iron in fig. 2.14(a,b). When the applied field is in the easy [010] direction as in fig. 2.14a, the domain saturated in that direction grows at the expense of the others. However in the hard [110] direction in fig. 2.14b, the process takes

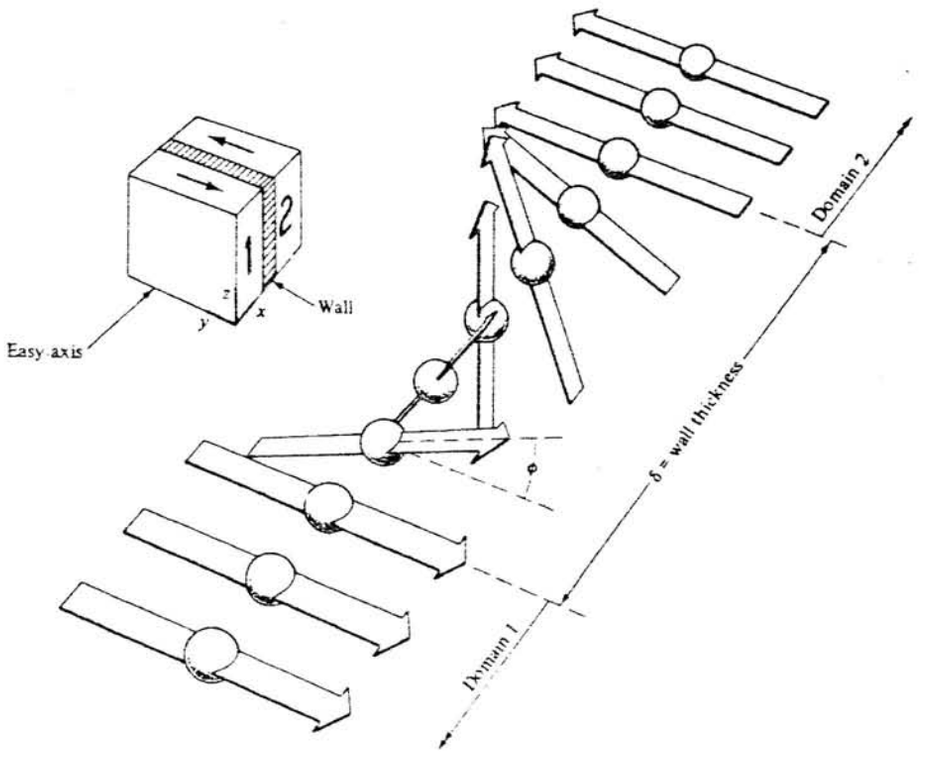


Fig. 2.12 Structure of a 180° domain wall.

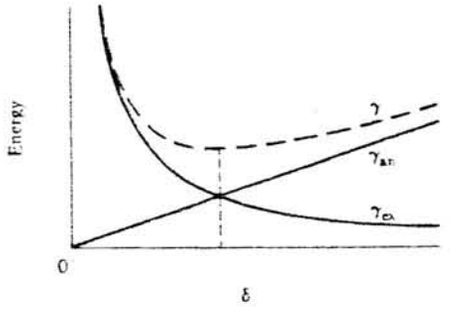


Fig. 2.13 Dependence of the total domain wall energy $\gamma$, on wall thickness $\delta$.

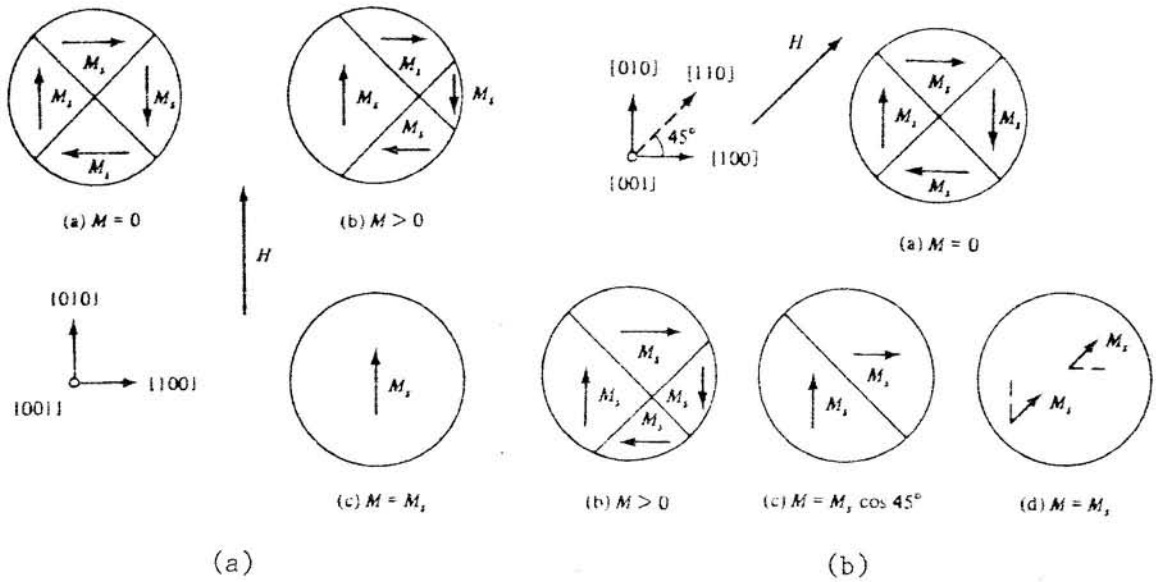


Fig. 2.14a,b Changes in domain structure a) parallel to the easy axis in iron, b) at 45° to the easy axis.

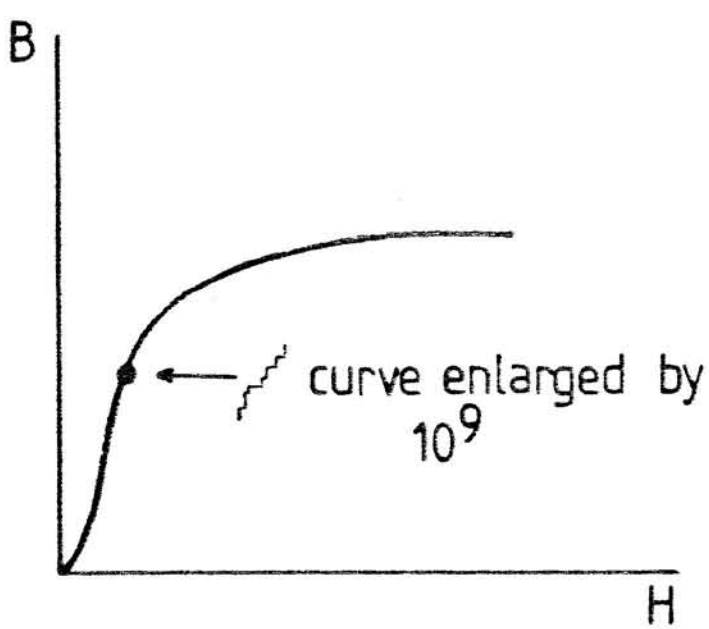


Fig. 2.15 The Barkhausen effect.

longer, because a new domain saturation magnetization direction has to be formed. This simple example shows the part that domains play in the magnetization process. The size of a domain depends on a balance between the magnetostatic energy and the domain wall energy.

### 2.5.4 Single Domain Particles

As discussed in Section 2.5, a single crystal will consist of many domains to minimise the magnetostatic energy. However, if the crystal is small enough a condition can be reached where it becomes a single domain, because the presence of a domain wall boundary will actually increase the total energy. Perfect, defect-free single domain particles cannot be easily demagnetized and since they have no domain wall to be moved by a field, their magnetization can only be reversed by rotation. Magnetic anisotropy, (usually crystal or shape anisotropy) impede magnetization rotation so it can be very difficult. Since useful permanent magnets are often produced from multidomain crystals, then some method is required that will stop domain walls from nucleating and moving thus maintaining a single direction magnetization.

### 2.5.5 Domain Wall Movement

In 1919 Barkhausen, set up an experiment whereby a search coil was wound on a specimen and connected through an amplifier to a loudspeaker. A noise occurred only during a change in magnetization on the steep part of the magnetization curve. The noise was due to the discontinuous motion of the domain walls

causing a magnetic induction change with time thus producing an emf in the coil; this is called the Barkhausen Effect and is illustrated in fig. 2.15.

In a polycrystalline material undergoing magnetization as illustrated in fig. 2.16, the initial part of the magnetization process involves a domain wall motion; at the "knee" of the magnetization curve a domain rotation occurs which requires a large field increase since work has to be done against the anisotropy forces. The contributions to this process are not readily separated, since both may occur in different regions of a specimen at the same time.

### 2.5.6 Domain Wall Processes

There are a number of scientific works discussing the domain processes taking place in real materials (see for example ref. 10). Basically, the two main processes are domain pinning and domain nucleation.

#### 2.5.6 I Domain Pinning

##### i Pinning by inclusions

Inclusions in the metallurgical sense include: second phase particles in a multi-component alloy; hard inclusions such as carbides or oxides; impurities or just cracks or holes. In terms of a magnetic point of view, inclusions may be regarded as a region of different or zero spontaneous magnetization.

When a domain wall bisects an inclusion such as from (a) to

(b) in fig. 2.17, the wall area will consequently decrease. If the radius of a spherical inclusion is r, then the wall area will decrease by $\pi r^2$ and the wall energy consequently decreases by $\pi r^2 \gamma$, where $\gamma$ is the total wall energy. An inclusion situated within a domain (see fig. 2.17c) will have free poles on it and an associated magnetostatic energy which forms a greater source of domain wall energy. However when the wall moves to (d), and bisects the inclusion, the free poles are redistributed as shown, and the magnetostatic energy is approximately halved.

Néel pointed out that the magnetostatic energy of an inclusion isolated within a domain could be decreased if subsidiary spike domains formed on the inclusion, and be reduced to zero by closure domains when a wall bisected the inclusion. In fig. 2.18 this effect is shown where the total free pole strength is spread over a larger surface as in fig. 2.18b than fig. 2.18a; and such a "dilution" decreases the magnetostatic energy. If a wall bisects an inclusion, the magnetostatic energy can be reduced to zero, at the cost of a little wall energy, if closure domains form as shown in fig. 2.18c.

When a wall passes through an inclusion under the action of an upward applied field, closure domains are dragged out in the direction of the passing domain wall, but only to a certain limit, otherwise too much wall energy would be added to the system. Eventually, the main wall jumps away from the dragged out domains, leaving spike domains attached to the inclusions. This is a Barkhausen jump and the process is shown schematically in fig. 2.19; it is reversible providing the field is strong enough

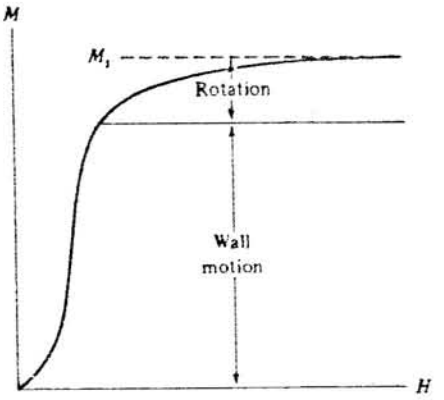


Fig. 2.16 Magnetization processes.

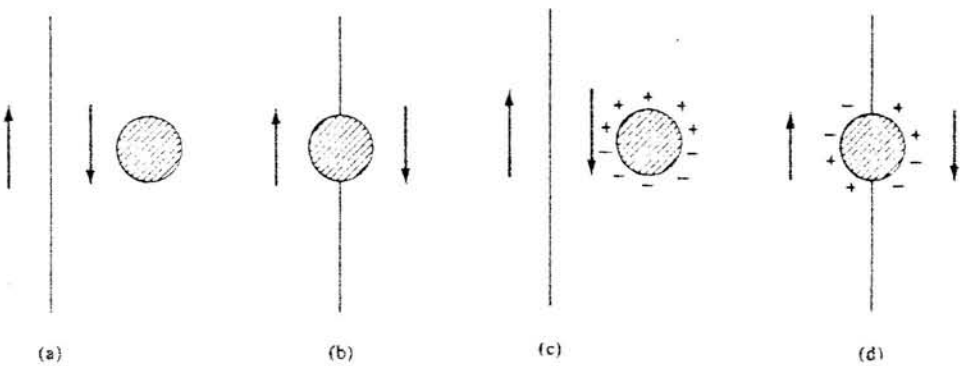


Fig. 2.17 Interactions of domain walls with inclusions.

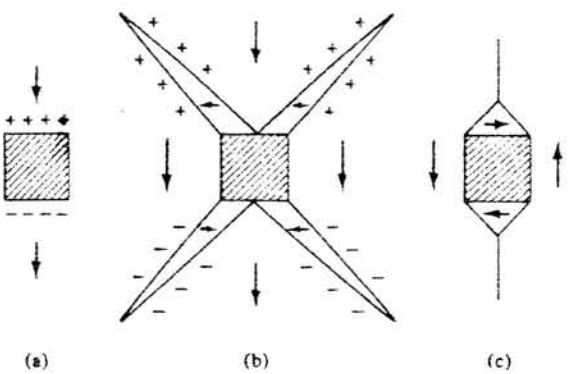


Fig. 2.18 Spike and closure domains on inclusions.

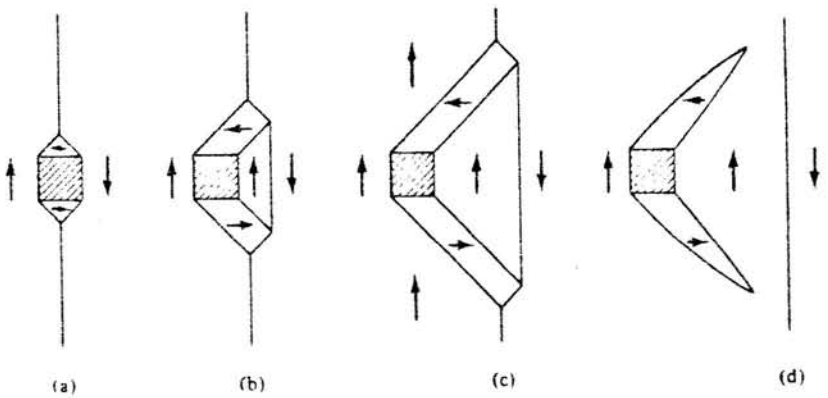


Fig. 2.19 Passage of a domain wall through an inclusion.

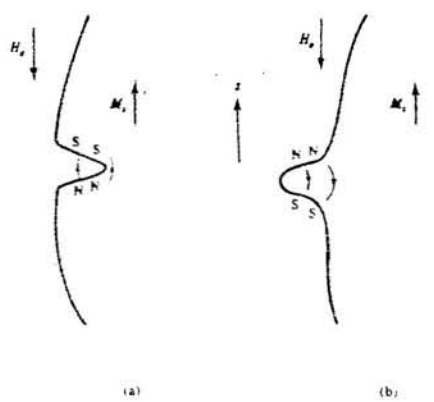


Fig. 2.20 Local fields near pits and bumps.

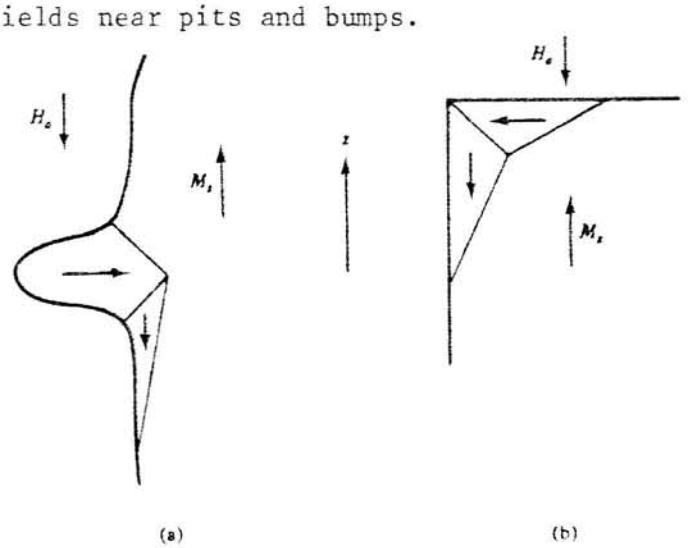


Fig. 2.21 Closure domains near pits and corners.

to move the wall to the left of the inclusion in fig. 2.19, resulting in spike domains pointing to the left. The domain pinning process in the "2:17" materials is discussed in detail in Chapter 4.

ii Pinning by microstresses

Microstresses can take the form of dislocations present in all specimens except in the most carefully grown single crystals or the presence of impurities in the material matrix. Microstresses impede domain wall motion because of magnetostriction. The magnetostriction force exerted on a microstressed region via a domain wall motion through this region, stores magnetoelastic energy, and it is this increase of energy of the system which can impede the movement of domain walls.

### 2.5.6 II Domain Nucleation

Regions of enhanced magnetization can also occur in a material. This can lead to a process of domain nucleation, whereby reverse domains move out from these regions causing a demagnetization. The processes of pinning and nucleation are both discussed in further detail in the next section.

### 2.5.7 Coercivity Mechanisms

The process of magnetization reversal involves the nucleation and motion of reverse domains. The coercivity can be controlled by a process predominantly dependent on the nucleation of reverse domain walls, or it can be dependent on the case of domain wall motion, where "pinning" plays the major role; alternatively, both

processes may be equally important. These two controlling factors have been developed theoretically to produce a wall nucleation dominated model (ref. 11) or a wall pinning controlled model (ref. 12). A more recent study of these mechanisms has been made by Livingston (refs. 10,13).

As stated earlier, below a critical size, a particle maintains a single domain structure. The only way for magnetization reversal to occur (ignoring shape anisotropy and assuming the particle is perfectly spherical) is by a rotation of the electron spin vectors. Therefore, the field required to reverse the direction of easy axis magnetization, is the crystal anisotropy field. Brown (refs. 7,8) suggested that the reversal field for a perfect, single domain, spherical and fully saturated crystal was, for a crystal of any size:

$$ {}_{i}H_{c} = \frac{2K}{M_{s}} \tag{2.8} $$

where ${}_{i}H_{c}$ is a particular value of the total field H acting on the crystal, H is the sum of the applied field $H_a$, and the demagnetizing field $H_d$; both acting opposite to the magnetization direction. In practice however, the fields required decrease as the particle size increases. This discrepancy for large particles between theory and experiment is called "Brown's Paradox". Since the coercivities of larger particles are much smaller than is expected from eqn. (2.8), the process of magnetization reversal cannot be caused by coherent rotation.

The process is one of a nucleation of reverse domains; in

a perfect crystal, this is just as difficult as rotation since it too requires a spin rotation. In real crystals however, imperfections can locally lower the energy for reverse domain nucleation.

The condition for wall nucleation in a single particle is:

$$H_a + H_d > \frac{2K}{M_s} \tag{2.9}$$

The presence of defects such as vacancies, interstitials or dislocations can locally change $M_s$ and K. If it decreases a consequent change in the anisotropy energy will facilitate the nucleation of domains. The most likely nucleators of reverse domains are surface defects which locally change the demagnetizing field $H_d$. Surface pits act to increase the magnetization as shown in fig. 2.20a; this is caused by the field at the base of the pit due to the poles on the pit walls which counteracts the field $H_a$. In fig. 2.20b a surface bump produces a local field which acts to demagnetize the particle and aid $H_a$; this process was pointed out by Kittel and Galt (ref. 14).

In fig. 2.21a a closure domain is shown near the bump; the closure domains form preferentially to lower the magnetostatic energy associated with the local field. This is also the case for sharp corners as shown in fig. 2.21b suggested by Shtrikman and Treves (ref. 15). In fact it has been postulated that reverse domains are already present at defects, so the nucleation process is one of "unpinning" walls that already exist.

Becker (ref. 16) gave further evidence for the role of surface imperfections as nucleating points by measuring coercivity before and after chemically polishing particles. He found that the coercivity was higher in the polished specimens than the untreated ones; this gave evidence to the idea that coercivity values are dependent on surface roughness. Becker (ref. 11) also found that the coercivity increased with increasing magnetizing fields. This is due to the fact that domains are driven more into irregularities as the magnetizing field increases and the energy required to unpin them is greater.

Defects play two roles as discussed by Livingston (ref. 13). On the one hand they can inhibit domain wall motion and so oppose the approach to saturation; or they can provide sites for heterogeneous nucleation of magnetization reversal and aid the approach to equilibrium saturation. Generally, large defects are most effective for the nucleation of domain walls, while small defects act ideally as pinning sites.

Whether the coercivity mechanism is one of domain wall nucleation or of wall pinning depends on the material itself. Single phase and two phase materials tend to be nucleation and precipitation controlled processes respectively, particularly in the rare earth magnet alloys as discussed by Livingston (ref. 10). In addition, grain boundaries can also have an effect on pinning domain walls depending on the grain boundary width (ref. 17), a pinning mechanism will occur if the exchange energy is locally lower in the grain boundary due to chemical changes. In fig. 2.22 the "virgin" demagnetization and magnetization curves are

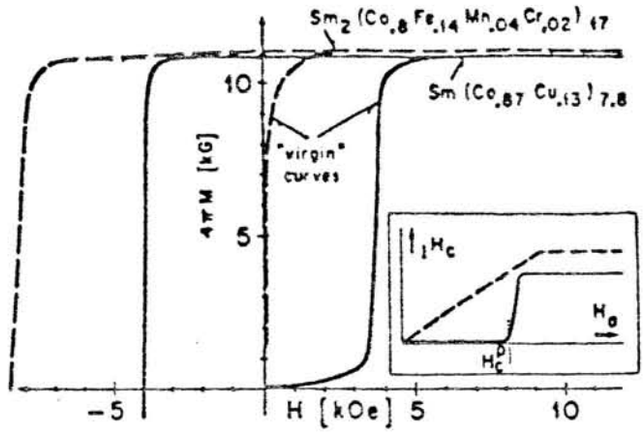


Fig. 2.22 "Virgin" magnetization and demagnetization curves for single phase (dashed-line) and two-phase (full-line) RE-Co magnets.

shown for a nucleation controlled (dashed line) and precipitation controlled process (full line). The full line is displaced relative to that for the nucleation dominated process because to magnetize a sample, energy is required to unpin the domain walls at second phase particles, whereas for the single phase material, the domain walls can move comparatively easily to be pinned at grain boundaries or free particle surfaces.

# CHAPTER THREE

## THE Sm-Co-TRANSITION METAL ALLOY SYSTEMS

### 3.1 Introduction

The Sm-Co-Transition Metal alloy systems form the basis of the rare-earth permanent magnet materials. It is necessary to consider the various phases that form in the Sm-Co-Transition Metal systems and their relevance to the magnetic properties. The rare earth - transition metal (RE - TM) alloys form a series of intermetallic compounds for which an extensive amount of work has been done in studying the various compositional ratios and magnetic characteristics (see for example refs. 18,19). It has been generally observed that the compounds of compositions: $RE_2Co_{17}$, $RE_2Co_7$, $RECo_3$ and $RECo_2$ exist with crystal structures based on the $CaCu_5$ type adopted by the $RECo_5$ compound.

The $RE_2Co_{17}$ intermetallic compound has been investigated by Khan (ref. 20) using X-ray diffraction techniques. He determined the crystal structures which consist of derivatives of the $CaCu_5$ form. The $CaCu_5$ structure has been investigated also for a range of $RETM_5$ alloys (TM = Transition Metal: Fe, Co, Ni, Mn) it was found (ref. 21) that all except those with Mn exhibited the $CaCu_5$ type structure.

## 3.2 The Samarium-Cobalt Binary System

The Sm-Co system has been investigated over the whole composition range using X-ray diffraction, thermoanalysis and metallography (ref. 22). The following compounds were observed: $Sm_3Co$, $Sm_9Co_4$, $SmCo_2$, $SmCo_3$, $Sm_2Co_7$, $SmCo_5$ and $Sm_2Co_{17}$. It was found that the mutual solubility of Sm and Co is small. Compounds in this system are known to possess structures derived from the $CaCu_5$-type structure; the differences arise from the different stacking sequences along the c-axis. The phase diagram after Buschow and Van der Goot (ref. 22) is shown in fig. 3.1.

More recently Nishio et al (ref. 23) have investigated Sm-Co alloys using thermomagnetic analysis, taking advantage of the different Curie temperatures of the alloys. They reported the possible existence of a $Sm_5Co_{19}$ phase which was indicated by a deflection in the magnetization versus temperature curve.

The types of structures occurring in the Sm-Co system for different compositions are summarised in table 3.1. Further descriptions may be found in a number of papers (see for example refs. 22,23,24,25).

## 3.3 The Copper-Samarium Binary System

Kuhn and Perry (ref. 26) have studied the copper-samarium system over the whole composition range using differential thermal analysis (DTA). They established the presence of two congruent phases, $Cu_6Sm$, $Cu_2Sm$ and three peritectic phases: $Cu_5Sm$, $Cu_4Sm$ and CuSm. In addition, eutectic reactions occur at 9 at.% Sm: 882°C, 28 at.% Sm: 818°C, and 71 at.% Sm: 597°C.

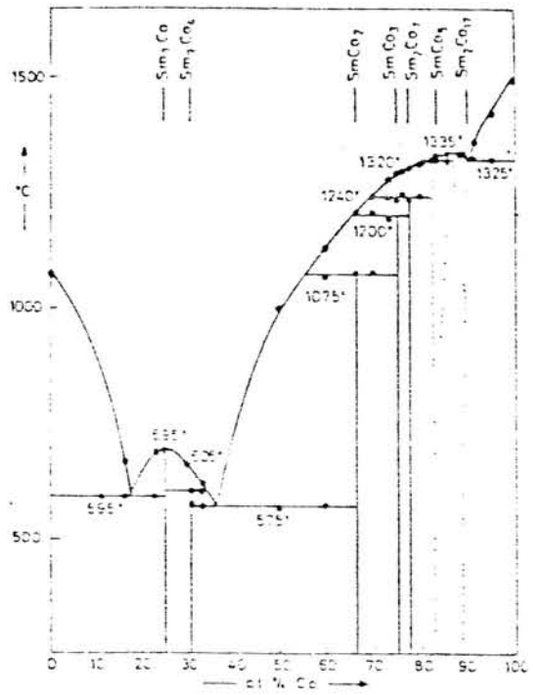

Fig. 3.1 Sm-Co phase diagram.

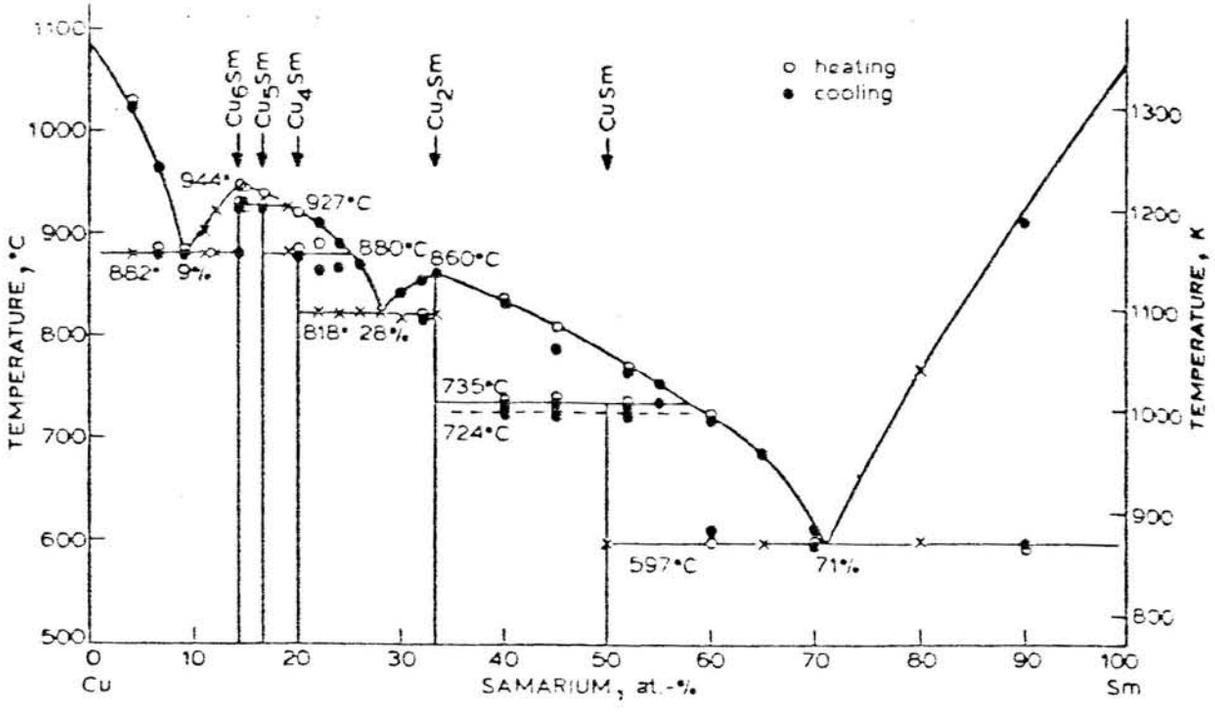


Fig. 3.2 Sm-Cu phase diagram.

Table 3.1 Sm-Co structure type across the whole composition range.

| Sm-Co Compound | Lattice Symmetry | Structure Type |
|---|---|---|
| $Sm_3Co$ | orthorhombic | $Fe_3C$ |
| $Sm_9Co_4$ | orthorhombic | |
| $SmCo_2$ | cubic | $MgCu_2$ |
| $SmCo_3$ | rhombohedral | $GdCo_3$ |
| $Sm_2Co_7$ | hexagonal | $Ce_2Ni_7$ |
| $SmCo_5$ | hexagonal | $CaCu_5$ |
| $Sm_2Co_{17}$ | α-rhombohedral<br>β-hexagonal | $Th_2Zn_{17}$<br>$Th_2Ni_{17}$ |

The experimental phase diagram is shown in fig. 3.2, based on DTA results, metallography and electron microprobe analyses. The system is divided into three subsystems, each bounded by a component metal or a congruently melting intermetallic phase.

## 3.4 The Samarium-Iron Binary System

Buschow (ref. 27) investigated the Sm-Fe system by X-ray diffraction, thermoanalysis and metallography. A tentative phase diagram was drawn from the X-ray data (see fig. 3.3) three compounds were observed: $SmFe_2$ ($MgCu_2$-type structure), $SmFe_3$ ($PuNi_3$-type) and $Sm_2Fe_{17}$ ($Th_2Zn_{17}$-type). Buschow indicated that unlike the Co and Ni-RE systems there were no $CaCu_5$-type compounds formed on alloying Fe with the RE metals.

## 3.5 The Samarium-Copper-Cobalt System

The Sm-Co-Cu system has been studied in the phase space between the 1:5 and 2:17 phases by various workers (refs. 28,29) who looked at metallographic changes along with DTA and electron probe microanalysis (EPMA). The compositions and heat treatments chosen were those known to be relevant to obtaining good magnetic properties (ref. 30).

The ternary phase diagram sections chosen by Perry (ref. 28) consisted of: isotherms at 1200°C and 800°C (see figs. 3.4a and 3.4b respectively); isopleths at 10 at.% and 20 at.% Cu (figs. 3.5a and 3.5b) and at a Sm:(Co + Cu) ratio of 1:6 (see fig. 3.6).

According to Nagel (ref. 29), metallographic investigations showed that single phase material was only obtained along the

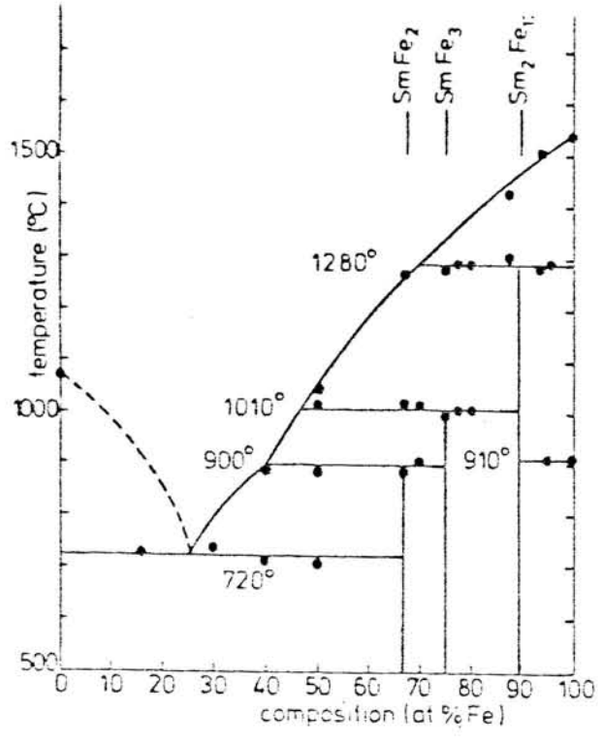


Fig. 3.3 Sm-Fe phase diagram

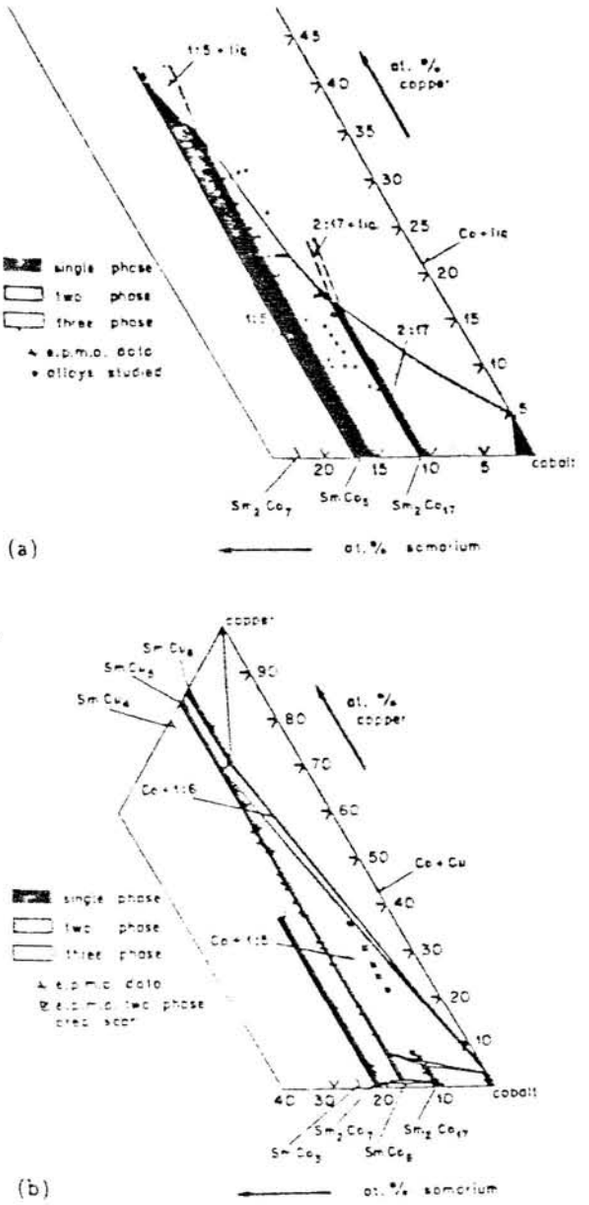


Fig. 3.4 Isothermal sections of the Sm-Co-Cu phase diagram at a) 1200°C, b)800°C.

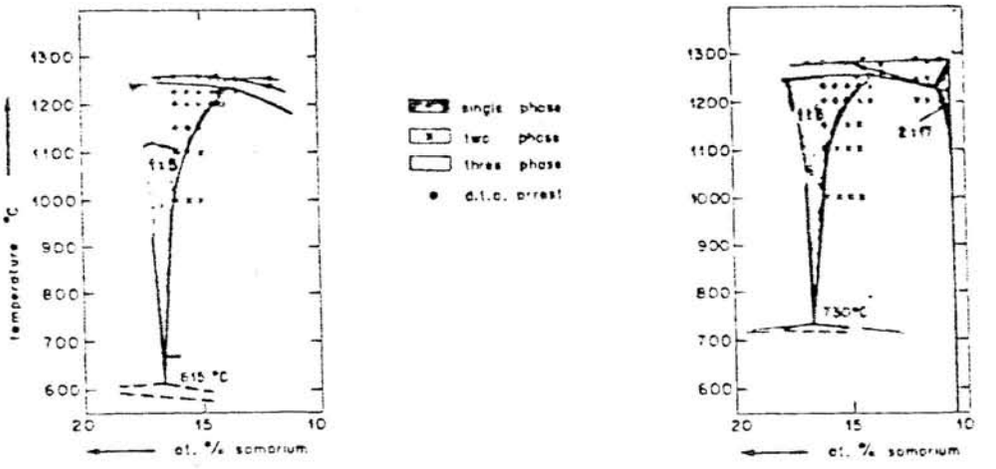


(a) (b)

Fig. 3.5 Isopleths at a) 10 at.% Cu and b) 20 at.% Cu

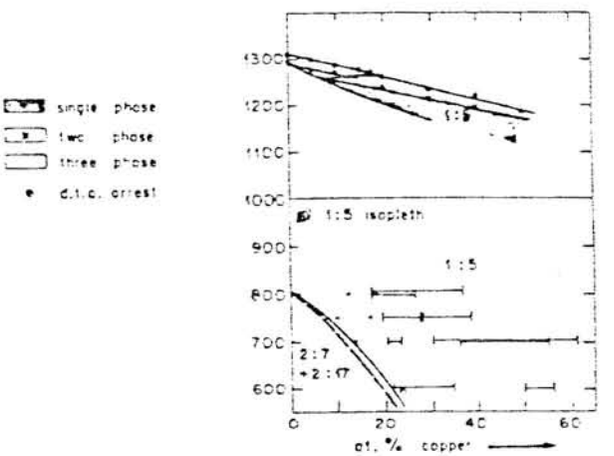


Fig. 3.6 Isopleth along a Sm: (Co + Cu) = 1:6 line

tie-line between $SmCo_5$ and $SmCu_6$ within a narrow composition range around $Sm_2Co_{17}$. Along this tie-line, quenching of the melts was necessary to avoid a eutectoid decomposition of the 1:5 phase into the 2:7 and 2:17 phases. Nagel also showed that the maximum copper solubility in $Sm_2Co_{17}$ for various $Sm_2(Co_{1-y}Cu_y)_{17}$ alloys was for y = 0.13. In the phase space between 1:5 and 2:17, the material formed at least two phases, with structures of the type 1:5 and 2:17.

Considering the work of Perry (ref. 28), the temperatures at which the 1:5 phase was observed extended well below the $SmCo_5$ eutectoid temperature. The binary eutectoid temperature depends on the copper content: it falls from 805°C to 600°C for 21 at.% Cu. The investigation also indicated a mutual solubility of the $SmCo_5$ and $SmCu_5$ phases down to at least 800°C.

The stability of the 1:5 phase increases with increasing copper content, and there is a widening of the homogeneity region as shown in figs. 3.5a and 3.5b. In addition, the 1:5 phase, as shown in the 20 at.% Cu isopleths in fig. 3.5b, changes from being formed peritectically to being the primary phase with the peritectic line changing to a eutectic trough.

In general, the 2:17 phase is repressed by the addition of copper. In fig. 3.4a, the 2:17 phase meets the solidus at about 16 at.% Cu in solution, whereas at 800°C only 4 at.% Cu can be dissolved. According to Perry the diffusion rates in 2:17 are markedly lower than in the 1:5 phase.

## 3.6 The Sm-Co-Cu-Fe System

Some work has been done on this alloy system (ref. 31), but at the present time no work has been undertaken in investigating the quarternary phase diagrams. Livingston and Martin (ref. 31) investigated an alloy of composition $Sm(Co_{0.8}Cu_{0.15}Fe_{0.05})_7$ using transmission electron microscopy. A sample quenched from 1200°C was found to be in the 1:5 type single phase condition. In samples aged at various times and temperatures it was generally found that a 2:17 type coherent phase appeared forming a cellular microstructure, this 2:17 type phase subsequently became incoherent on further ageing.

## 3.7 Crystal Structures of RE-Co Alloys

### 3.7.1 Introduction

In table 3.2 the various crystal structures observed in the binary RE - TM systems are given. The compositions: $RETM_5$, $RE_2TM_{17}$ and $RE_2TM_7$ are important in that alloys of these types exhibit superior magnetic performance. Therefore their crystal structures will be discussed in the following sections.

### 3.7.2 $RETM_5$ Compounds

#### i) Crystal Structure

$RETM_5$ compounds have a $CaCu_5$ type crystal structure (ref. 32) as shown in fig. 3.7. Large deviations from stoichiometry may occur (ref. 33), whereby the rare earth atoms are replaced by pairs of cobalt atoms.

Table 3.2 Survey of Rare Earth - Transition Intermetallic Structures.

| Compound | Lattice Symmetry | Structure Type | TM |
|---|---|---|---|
| $RE_3TM$ | Orthorhombic | $Al_3Ni$ | Ni, Co |
| $RE_4TM_3$ | Hexagonal | $Ho_4Co_3$ | Co |
| $RE_2TM_{1.7}$ | Hexagonal | $Pr_2Co_{1.7}$ | Co |
| RETM | Orthorhombic | FeB or CrB | Ni |
| $RETM_2$ | Cubic | $MgCu_2$ | Ni, Co, Fe |
| $RETM_3$ | Hexagonal | $CeNi_3$ | Ni |
| | Rhombohedral | $PuNi_3$ | Ni, Co, Fe |
| $RE_2TM_7$ | Hexagonal | $Ce_2Ni_7$ | Ni, Co |
| | Rhombohedral | $Gd_2Co_7$ | Ni, Co |
| $RE_5TM_{19}$ | Rhombohedral | $Pr_5Co_{19}$ | Co |
| $RE_6TM_{23}$ | Cubic | $Th_6Mn_{23}$ | Fe |
| $RE_5TM$ | Hexagonal | $CaCu_5$ | Ni, Co |
| | Hexagonal | $Th_2Ni_{17}$ | Ni, Co, Fe |
| $RE_2TM_{17}$ | Rhombohedral | $Th_2Zn_{17}$ | Ni, Co, Fe |
| $RETM_{13}$ | Cubic | $NaZn_{13}$ | Co |

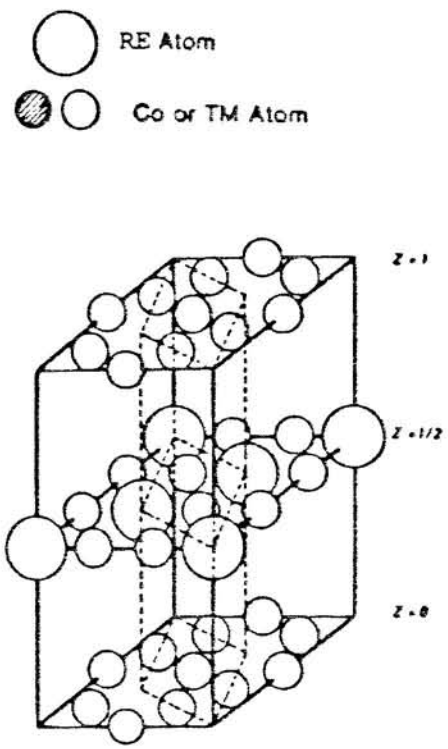


Fig. 3.7 Hexagonal $CaCu_5$-type crystal structure.

ii) Stability of the $RETM_5$ Structure

Buschow and Goot (ref. 34) found that the homogeneity region around the compound $RECo_5$ increased as the rare earth metal radius decreased. The deviations give rise to an entropy contribution to the free energy and at high temperatures this contribution will be large and thus stabilizes the $CaCu_5$ type structure; this may explain why some of the $RECo_5$ compounds decompose on cooling.

The RE atoms are much larger than the Co atoms in the $CaCu_5$ structure type and the size of the RE atoms determines the length of the c-axis (see fig. 3.8a). The addition of cobalt atoms as in the case of $SmCo_{5.86}$ (ref. 34), causes the cobalt atoms to take up new positions on the ligand in the unit cell and the c-axis length will consequently increase. If 30-35% of the cobalt atoms are substituted in the $CaCu_5$ type structure of a $RECo_5$ compound, then an ordered structure of the type $Th_2Ni_{17}$ is obtained (see fig. 3.8b).

It is probable that the presence of cobalt atoms on the ligand in $RE_2Co_{17}$ structures is responsible for the lower crystal anisotropy and coercive force of these compounds compared to the $RECo_5$ compounds (ref. 35).

3.7.3 $RE_2TM_{17}$

i) Crystal Structure

Alloys of the $RE_2TM_{17}$ composition can crystallize in two forms: the $\alpha$, rhombohedral $Th_2Zn_{17}$ type structure; the $\beta$, hexagonal $Th_2Ni_{17}$,

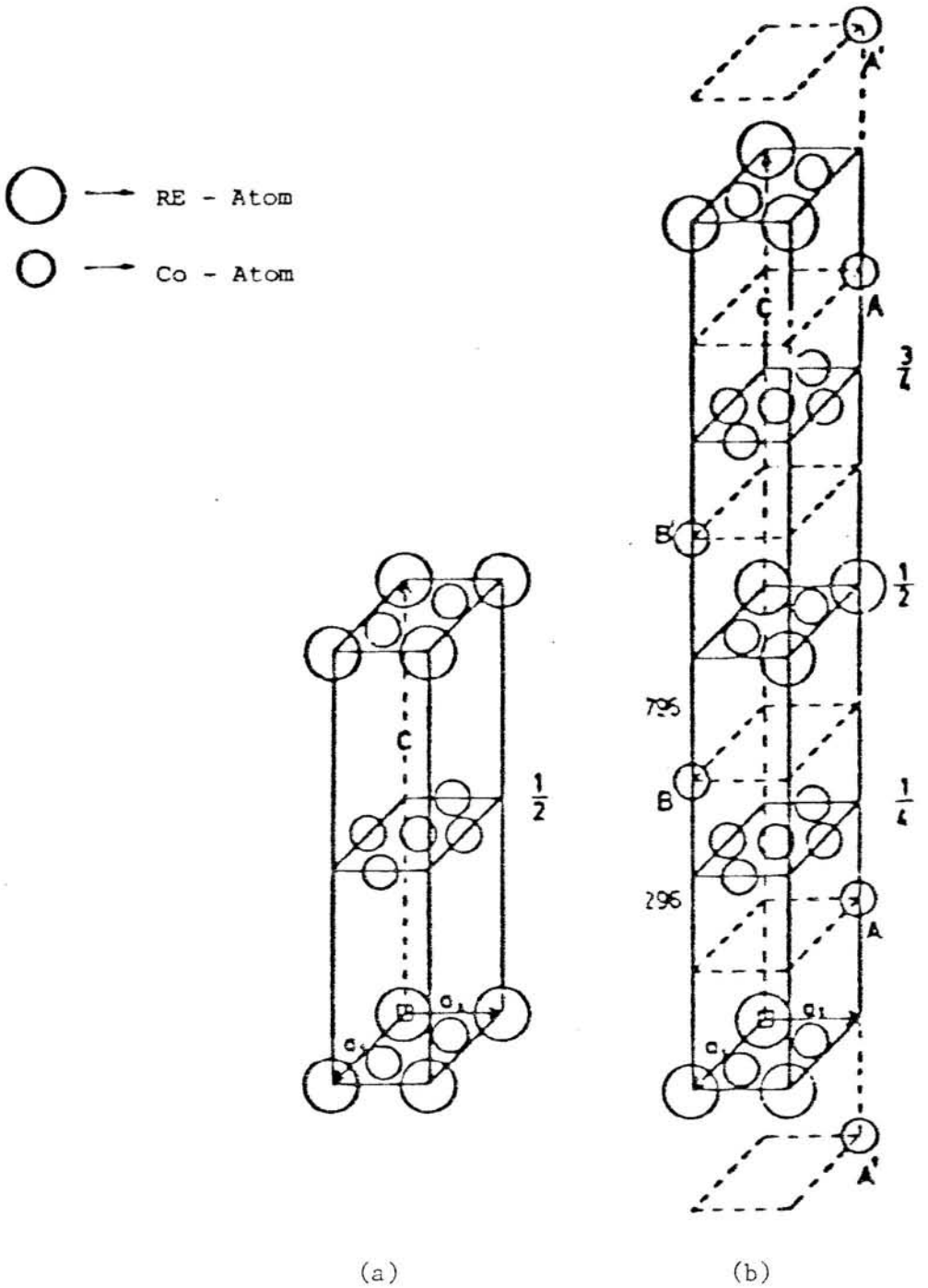


Fig. 3.8 (a) Unit cell of the structure of the stoichiometric $AB_5$ compound of the $CaZn_5$-type.

(b) $\frac{1}{3}$ of the unit cell of the structure of the $A_2B_{17}$ compound of the $Th_2Ni_{17}$-type.

both structures are shown in fig. 3.9a, b.

The stacking sequence of the two $RE_2TM_{17}$ type structures can be explained by considering fig. 3.10b; here, the $RETM_5$ is built up of two layers. In the top layer both RE and TM atoms are found, in the next layer only TM atoms are present. Fig. 3.10a shows an expanded view of the first layer containing both RE and TM atoms, here ABCD indicate the basal plane of the unit cell of edge a. Therefore, if in the basal plane, the replacement occurs at site (A), it will occur at site (C) in the next layer containing RE atoms. In the following layer it may either occur at site (C), leading to a hexagonal structure or at site (E) leading to a rhombohedral structure.

Therefore, the form of the two $RE_2TM_{17}$ structures is made up of different stacking sequences of the $RETM_5$ subcells as shown in fig. 3.11. The hexagonal form consists of a stacking sequence ABAB... , while the rhombohedral form is of the stacking sequence ABCABC... .

ii) Stability of the $RE_2TM_{17}$ Structure

The conditions favouring the formation of the $\alpha$ or $\beta$ forms were investigated by Buschow (ref. 36). Samples were prepared by either splat cooling after melting in an arc furnace or heating to the required temperature and then quenching after maintaining the specimens at this temperature for one hour. Buschow's results for the lattice parameters of the $RE_2Co_{17}$ specimens are shown in table 3.3 for decreasing outer radius of the rare earth elements. It may be seen from table 3.3 that

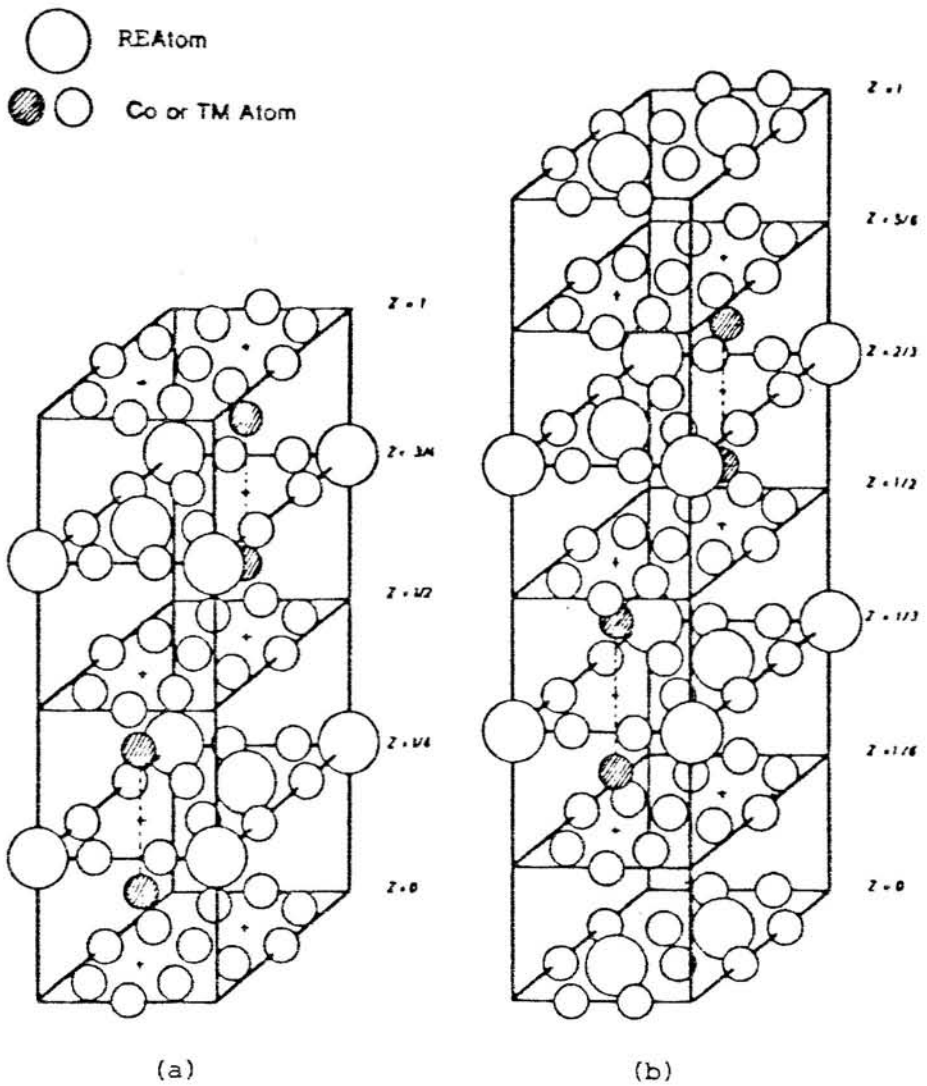


Fig. 3.9 Crystal structures of the $RE_2TM_{17}$-type compounds with (a) hexagonal modification ($Th_2Ni_{17}$-type) and (b) rhombohedral modification ($Th_2Zn_{17}$-type).

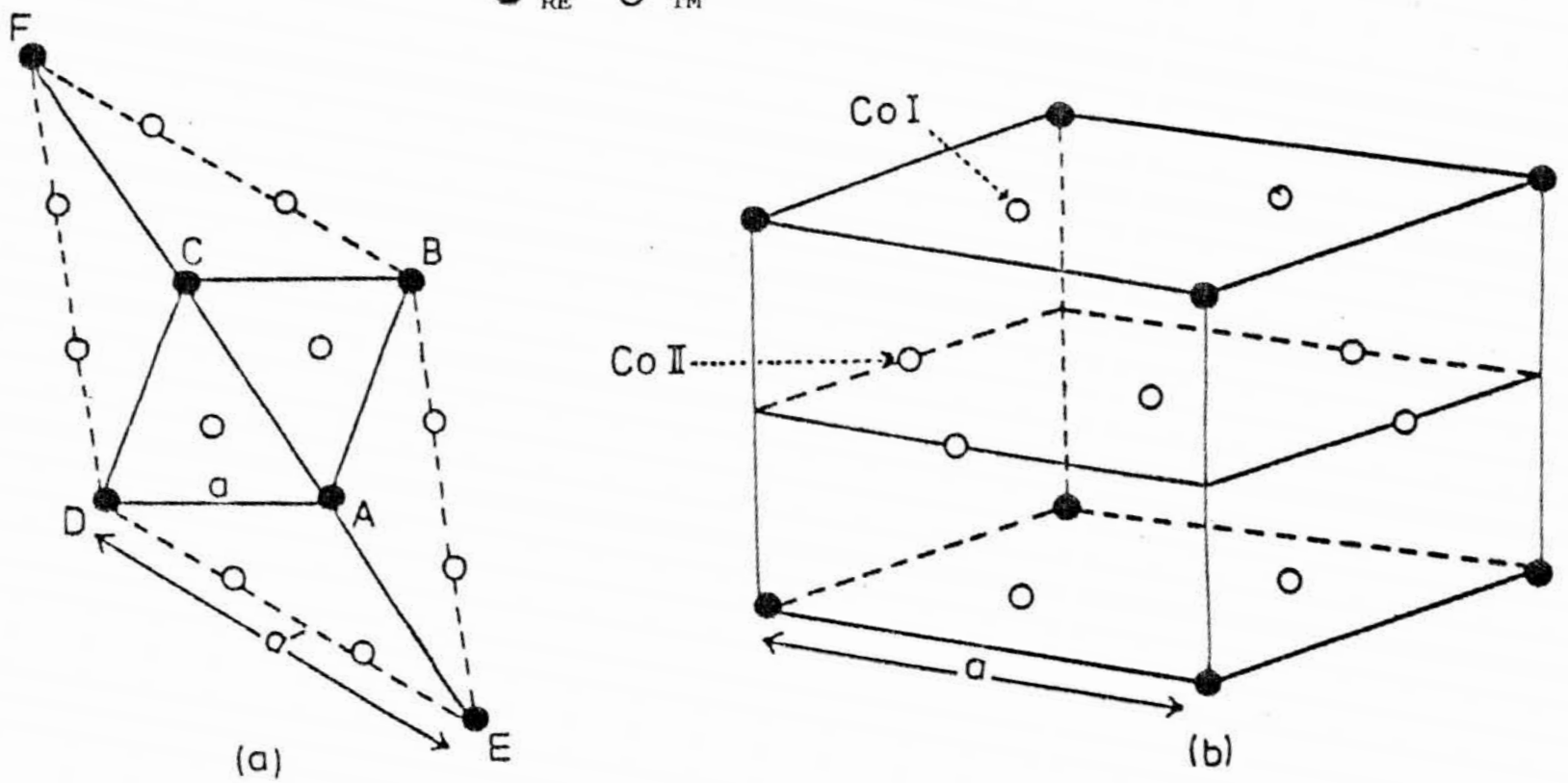


Fig. 3.10 . (a) Position of atoms in a plane perpendicular to the c-direction of the $RETM_5$ lattice.

(b) Unit cell of the $RETM_5$ structure type.

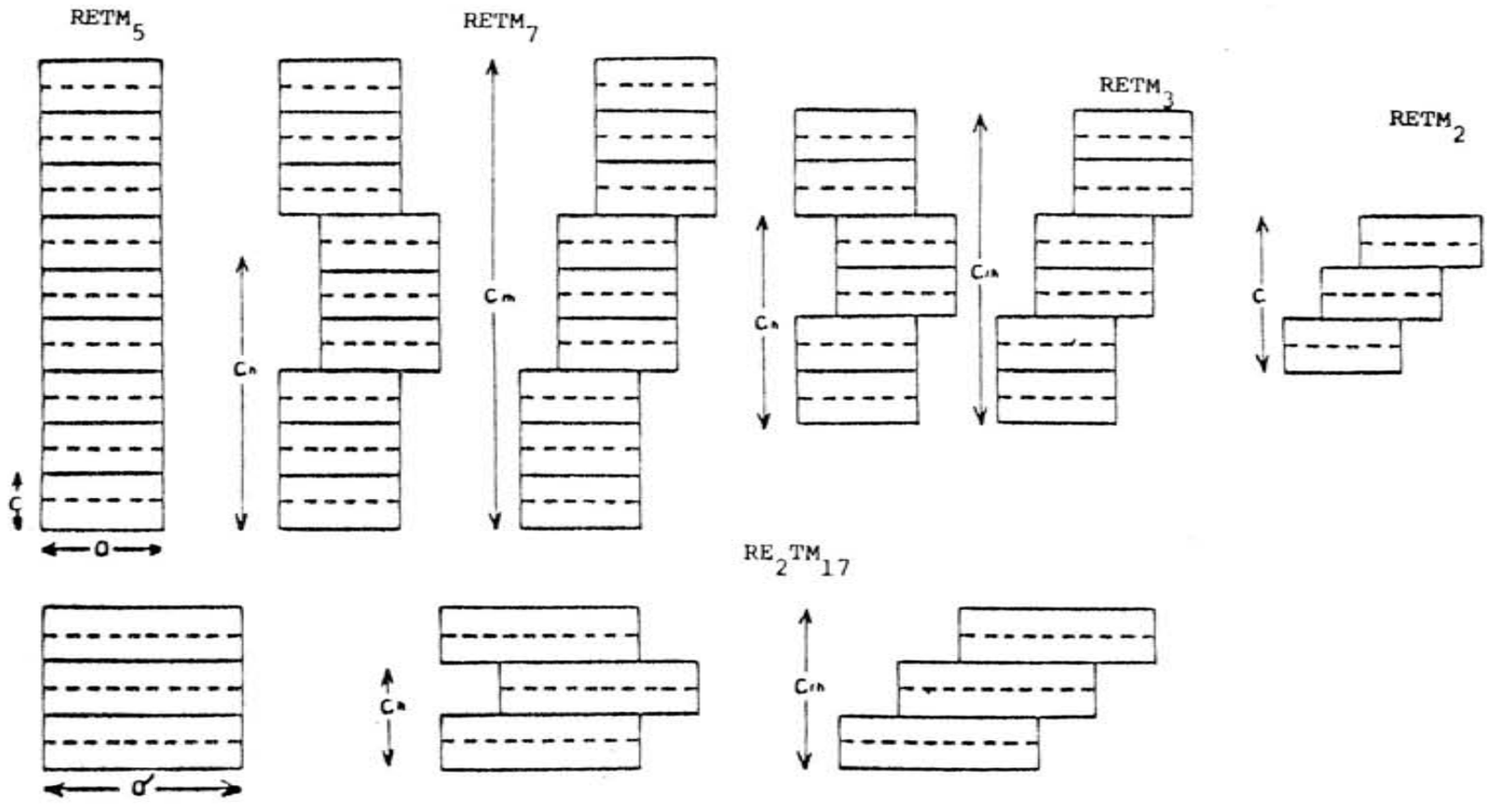


Fig. 3.11 Schematic representation of the stacking modes for the various RETM structures.

TABLE 3.3 Lattice Parameters of the $RE_2Co_{17}$ Compounds.

| Compound | $Th_2Zn_{17}$ type (Rhombohedral) | | $Th_2Ni_{17}$ type (Hexagonal) | | |
|---|---|---|---|---|---|
| | Lattice Constants | | Lattice Constants | | |
| $Ce_2Co_{17}$ | 8.370 | 12.193 | 8.371 | 8.136 | S |
| $Pr_2Co_{17}$ | 8.427 | 12.265 | | | |
| $Nd_2Co_{17}$ | 8.407 | 12.257 | | | |
| $Sm_2Co_{17}$ | 8.379 | 12.212 | 8.360 | 8.515 | S |
| $Gd_2Co_{17}$ | 8.365 | 12.184 | 8.351 | 8.125 | S |
| $Tb_2Co_{17}$ | 8.344 | 12.19 | 8.348 | 8.125 | W |
| $Y_2Co_{17}$ | 8.344 | 12.19 | 8.341 | 8.125 | W |
| $Dy_2Co_{17}$ | 8.31 | 12.07 | 8.328 | 8.125 | |
| $Ho_2Co_{17}$ | | | 8.320 | 8.113 | |
| $Er_2Co_{17}$ | | | 8.310 | 8.113 | |

S:- samples quenched by splat cooling.

W:- samples quenched in water.

the heavier RE compounds favour the $Th_2Ni_{17}$ hexagonal structure, which becomes less stable with increasing atomic radius of the RE component. $Sm_2Co_{17}$ has the hexagonal $Th_2Ni_{17}$ structure when splat cooled and the rhombohedral $Th_2Zn_{17}$ structure when water quenched. Buschow and den Broeder (ref. 25) confirmed that for the homogeneity regions of $Gd_2Co_{17}$ and $Sm_2Co_{17}$, the $Th_2Zn_{17}$ type structure was associated with the RE rich side, and the $Th_2Ni_{17}$ type with the Co rich side.

iii) Summary

There are three general factors affecting the final structure adopted by the $RE_2TM_{17}$ alloys: (1) the size of the RE atom; (2) the cooling rate of the alloy melt; (3) the compositions within the boundary region.

### 3.7.4 $RE_2TM_7$ Compounds

i) Crystal Structure

At this compositional ratio, the light rare earths adopt the hexagonal $Ce_2Ni_7$ type structure (ref. 24). The heavier rare earths adopt the $Gd_2Co_7$ type (ref. 37) which is rhombohedral. Both these structures are derived from the $RETM_5$ structure ($CaCu_5$ type) by the substitution of TM with RE atoms. The stacking sequence is shown in fig. 3.11.

ii) Stability of the $RE_2TM_7$ Structure

An annealed sample of $La_2Co_7$ consists of the hexagonal

$Ce_2Ni_7$ structure type, according to Buschow and Velge (ref. 38), however if quenched from the liquid state the samples crystallize in the rhombohedral, $Gd_2Co_7$ type structure. At high temperatures, it has been suggested that $La_2Co_7$ has the $Gd_2Co_7$ type structure and on cooling becomes unstable and transforms to the $Ce_2Ni_7$ structure. This is true for $Ce_2Co_7$, $Pr_2Co_7$, $Nd_2Co_7$ and $Sm_2Co_7$ (ref. 39) all of which transformed from the high temperature rhombohedral $Gd_2Co_7$ to the hexagonal $Ce_2Ni_7$ structure on cooling.

# CHAPTER FOUR

# RARE EARTH COBALT PERMANENT MAGNETS

## 4.1 Introduction

Besides the ferrites and alnicos the rare earth cobalt (RE-Co) permanent magnet (PM) alloys, belong to the most widely used PM materials. The history of the development of the RE-PMs has been characterised by attempts to attain high energy products, and at the same time to reduce raw material costs. The result of this is a broad range of commercially available RE-PM materials, for which several reviews have appeared (see for example ref. 40).

The RE-TM (TM = transition metal) compounds are magnetically highly anisotropic; the theoretical value for coercivity is represented by the anisotropy field value as discussed in Section 2.5.7, which corresponds to a coherent rotation of the magnetization in perfect single domain particles situated in an applied field (ref. 7). The actual coercivity values are much smaller in fact, due to imperfections in real crystals; thus the coercivity mechanism is governed by the applied field required to create a nucleus of reverse domains or the field required to unpin domain walls from various pinning sites.

The magnetism of the RE-PM alloys are the result of large magnetic 4f-3d interactions which result in a large magnetic anisotropy and also the 3d exchange interactions which maintain

the magnetic ordering to above room temperature (ref. 41). The requirements for a material to have useful magnetic properties are generally that:

i) the compound must be ferri- or ferromagnetic with a relatively high Curie temperature (> 400°C)

ii) in the case of the RE-TM alloys the material must have a high uniaxial magnetocrystalline anisotropy, so the crystal structure must be non-cubic

iii) the room temperature saturation must be high (> 6000 G).

## 4.2 The "1:5" Type RE-Co Magnets

The historical development of the 1:5 type PMs and RE-Co magnets in general, began in 1966 when Hoffer and Strnat (refs. 42,43) measured the crystal anisotropy of the $YCo_5$ and $Y_2Co_{17}$ alloys. It was found that $YCo_5$ could be a useful magnetic material as it had an easy c-axis magnetization direction. According to a historical survey given by Strnat (ref. 44), before 1966, workers of the Naval Ordnance Laboratory prepared powders of $GdCo_5$ with a coercive force of 8 KOe.

It was soon realised that the material with the best handling properties was $SmCo_5$ (ref. 44). A polymer bonded magnet was reported in 1967, but to attain better energy products, the packing density had to be increased. It was thought that sintering would increase the density but all early attempts failed to produce a sintered magnet.

The starting point for the industrial production of Sm-Co magnets began in 1969 when Das (ref. 45) of the Raytheon Company announced that he had found a way of sintering $SmCo_5$ and had produced a magnet with an energy product of 20 MGOe. In fig. 4.1 plots are shown of the laboratory achievements in magnetic properties against time for the early RE-Co work. In 1973, a process was announced for the production of Sm-Co alloys in powder form directly from RE-oxides (ref. 46). This process bypassed several production steps and made possible a decrease in alloy costs. The process was called the reduction diffusion (R-D) process (ref. 47), and is summarised below, whereby a RE-oxide is mixed with other materials under an inert hydrogen atmosphere to form a $SmCo_5$ powder alloy:

$$10Co + RE_2O_3 + CaH_2 \rightarrow 2Co_5REO + CaO + H_2 \quad (850^oC)$$

$$2Co_5REO + 2CaH_2 \rightarrow 2Co_5RE + 2CaO + 2H_2 \quad (1050^oC)$$

The process produces powders ready for milling, however, the alloy tends to contain a higher proportion of oxygen and calcium than alloys produced by vacuum induction melting.

The drawback with the 1:5 type magnets is the raw material cost, and this has led to other developments in the area of (RE-TM) permanent magnets.

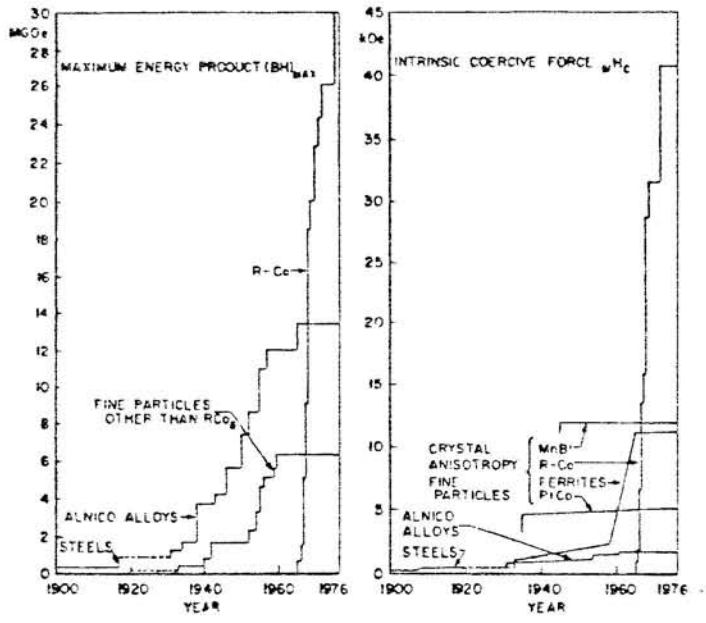


Fig. 4.1 The development of $_iH_c$ and $BH_{max}$ with time of various PM alloys.

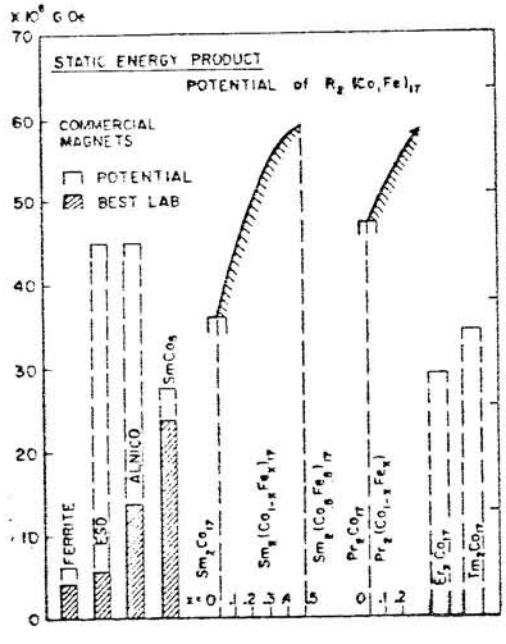


Fig. 4.2 $BH_{max}$ values for various $Re_2(Co,Fe)_{17}$ alloys.

## 4.3 The "2:17" Type RE-Co Magnets

### 4.3.1 Development of the "2:17" Magnets

The "2:17" magnetic alloys can be characterized by the coercivity mechanism; the formation of precipitates during a post solid solution heat treatment, inhibits the motion of domains by a pinning mechanism.

The "2:17" materials have a general composition $RE(Co,TM)_z$. RE stands for one or more rare earth metals, TM for a combination of transition metals including copper and z lies between 6 and 8.5.

The potential of the 2:17 alloys was realised very early on (ref. 44). These alloys are interesting because of their high potential remanences which are comparable to, or better than, the best alnico type magnets. However the anisotropy fields of the 2:17 compounds are rather low as compared to that of $SmCo_5$, and the main problem in the development of the 2:17 magnets has therefore been to increase the coercivity of the magnets to an acceptable level. Strnats' initial forcast (refs. 43,44) for the possibility of a second generation of RE-PMs was based on intermetallic phases of the type $RE_2(Co,Fe)_{17}$. The compounds with samarium as the principal RE component were found to have the most attractive combination of saturation magnetization, Curie temperature, magnetocrystalline anisotropy, environmental stability, cost per unit energy product and mechanical strength. Fig. 4.2 compares the theoretically possible energy products with these alloys to those achieved with other magnet types.

Fig. 4.3 shows the effect of compositions on the anisotropy directions for various 2:17 alloys.

In 1976 workers in Japan (ref. 48) and Switzerland (ref. 49) prepared sintered Sm(Co,Fe) alloys of 1:8 and 2:17 stoichiometry respectively, that were modified with other transition elements and achieved energy products of over 30 MGOe and intrinsic coercivities of between 7 and 10 KOe. The first 2:17 magnets appeared on the market in 1977 (ref. 50), the coercivity was increased by adding various elements from both the 3d and 4d groups, and by a post sintering annealing consisting of several steps. Recent work has involved investigating in detail, effects of heat treatments, microstructure and composition on the magnetic properties of these alloys (see for example, refs. 51, 52,53).

### 4.3.2 Magnets Based on the Composition $Sm_2(Co,Cu,Fe,M)_{17}$ (M = Zr, Ti, Hf, Ni, Mn, Cr, Nb, V)

As mentioned in the previous section, the 2:17 alloys developed from a need to increase magnetic properties while attempting to replace samarium and cobalt by lower priced and more readily available elements. Early work involved investigations into the effects of iron additions in the system $Sm_2(Co_{1-x}Fe_x)_{17}$ (ref. 54), and the effects of copper additions (ref. 31). Later work looked at the effects of adding Mn, Cr, Zr, Nb, Ti, Hf and Ni. Attempts have also been made to partially or wholly substitute samarium with cerium metal (ref. 55) which is cheaper and more readily available.

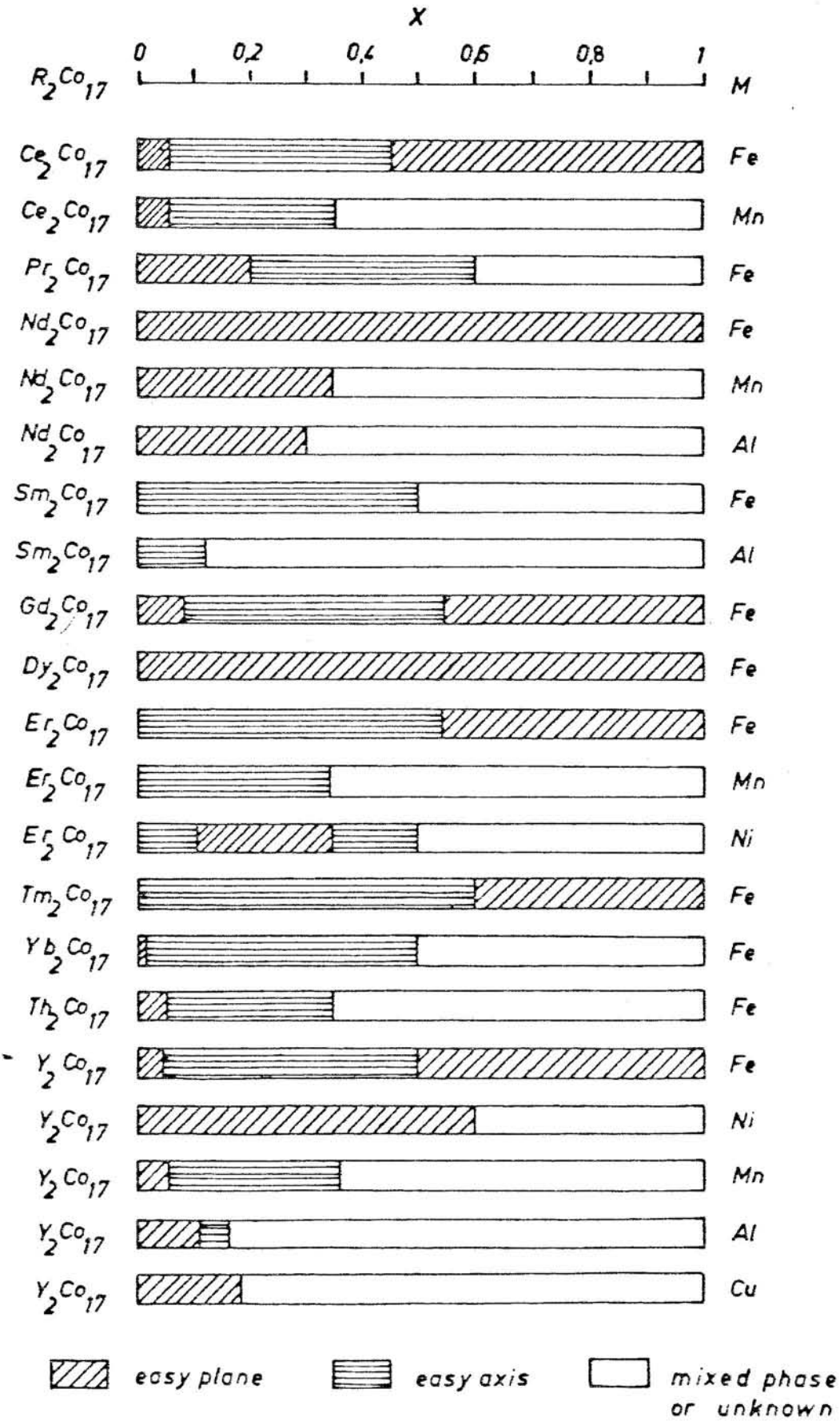


Fig. 4.3 The dependence of anisotropy direction on composition for $RE_2(Co_{1-x}M_x)_{17}$-type alloys.

Table 4.1

The magnetic properties of a range of "2:17"-type alloys.

| Composition | $(BH)_{max}$ [kJ/m$^3$] | $B_r$ [T] | $_JH_c$ [kA/m] | Reference |
|---|---|---|---|---|
| 1. $Sm(Co_{0.85}Fe_{0.05}Cu_{0.1})_8$ | 176 | 1.02 | 850 | (16) |
| 2. $Sm(Co,Fe,Cu,Cr)_{8.5}$ | 240 | 1.12 | 520 | (3) |
| 3. $Sm(Co_{0.8}Fe_{0.075}Mn_{0.125})_{8.5}$ | 223 | 1.09 | 1070 | (18) |
| 4. $Sm(Co_{0.73}Fe_{0.13}Cu_{0.14})_7$ | 188 | 0.97 | 560 | (30) |
| 5. $Sm(Co_{0.76}Fe_{0.1}Cu_{0.14})_{6.8}$ | 211 | 1.04 | 502 | (31) |
| 6. $Sm(Co_{0.69}Fe_{0.2}Cu_{0.1}Zr_{0.01})_{7.4}$ | 240 | 1.12 | 535 | (2, 17) |
| 7. $Sm(Co_{0.73}Fe_{0.12}Cu_{0.14}Ti_{0.01})_7$ | 172 | 0.93 | 760 | (32) |
| 8. $Sm_{0.75}Ce_{0.25}(Co_{0.81}Fe_{0.04}Cu_{0.15})_{7.2}$ | 161 | 0.92 | 416 | (15) |
| 9. $Ce(Co_{0.73}Cu_{0.14}Fe_{0.12}Ti_{0.01})_{8.5}$ | 104 | 0.94 | 488 | (4) |
| For comparison: $SmCo_5$ | 192 | 0.98 | > 2000 | (19) |

These developments, in terms of investigating the effects of composition on the magnetic properties have led to a range of 2:17 RE-Co PM alloys. In table 4.1, the magnetic properties of representative 2:17 magnet alloys are shown to indicate the range of compositions that have been investigated. In fig. 4.4 the progress of the development of the magnetic properties are shown.

i) The Effect of Copper Additions on Magnetic Properties

Recent work has looked at the effects of Cu additions on the pinning mechanism of the precipitates in 2:17-type alloys (ref. 56). Livingston (ref. 57) found that the addition of copper facilitates the generation of a fine scale precipitate structure by decreasing the c-axis misfit between the 1:5 phase and 2:17 matrix. Nagel and Menth (ref. 58) studied the influence of Cu content on the magnetic properties of a $Sm_2(Co,Cu)_{17}$ compound and found that the pinning of domains was due to $Sm(Co,Cu)_5$ precipitates in a 2:17-type matrix, for the alloy composition studied. The pinning occurred because the domain wall energy in the 1:5 phase was only a fifth of that for the matrix so that domain walls would preferentially lie in the 1:5 precipitates. It was also suggested that copper decreases the c-axis misfit between the phases and this favours the precipitates orientating along the c-axis, improving the conditions for pinning.

Potenziani (ref. 56) concluded that copper additions degrade the magnetic properties of the 1:5 precipitates which then act as a barrier to domain wall motion, suggesting that energetically

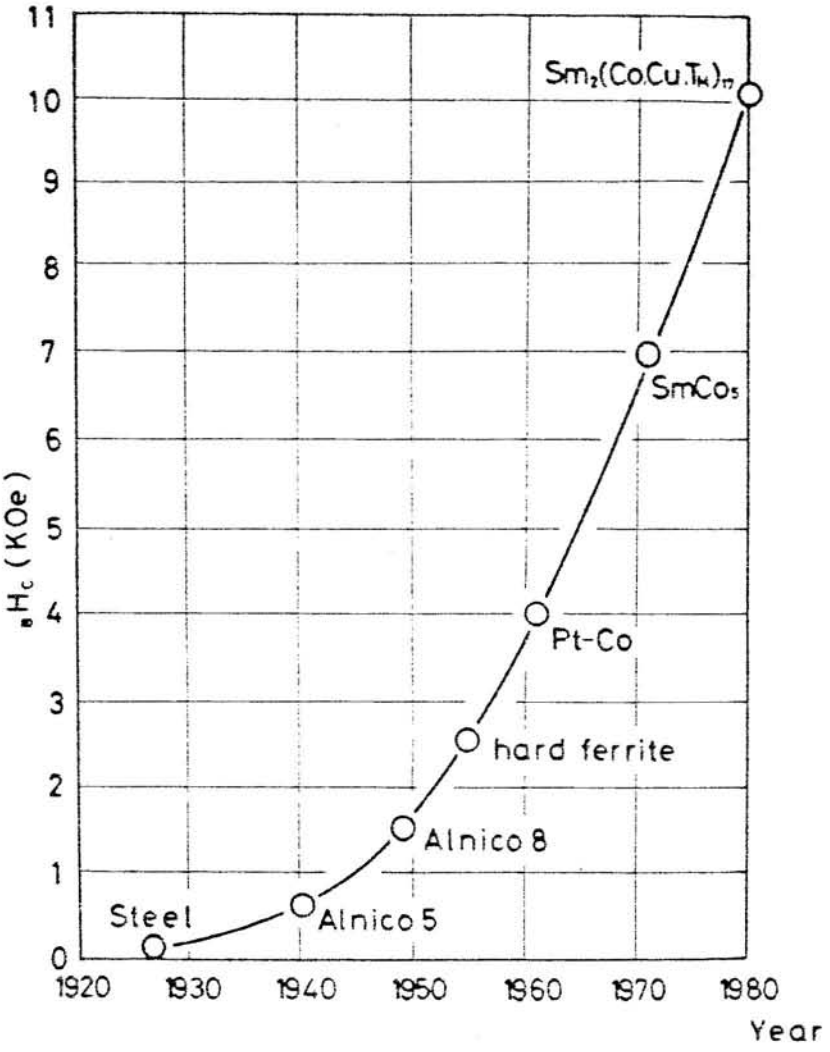


Fig. 4.4 The progress of PMs before the appearance of Nd-Fe-B alloys.

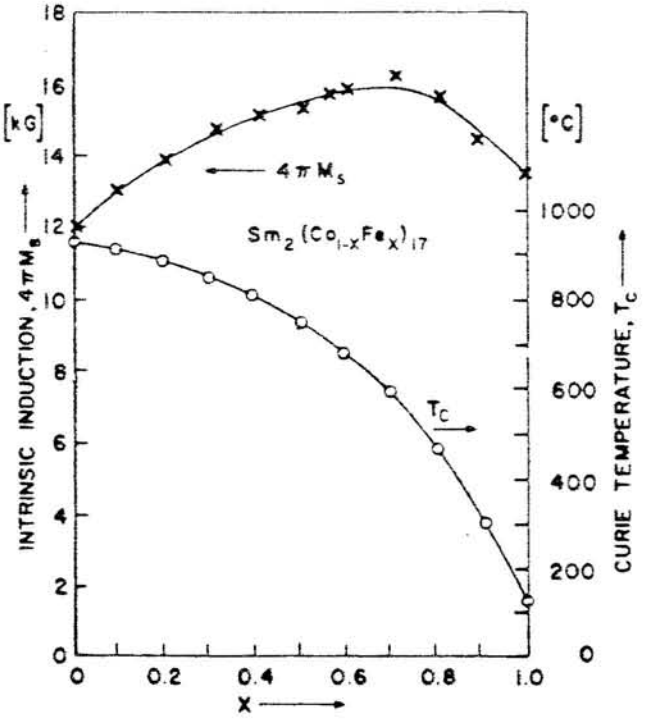


Fig. 4.5 Room temperature values of the intrinsic induction of 20 kOe and the Curie Temperature for a $Sm_2(Co_{1-x}Fe_x)_{17}$ alloy.

domains prefer to lie in the precipitates. It was proposed that the copper replaces the TM atoms of the 1:5 phase, thus increasing the difference between the magnetic anisotropies of the 1:5 and 2:17 phases. This idea was reinforced by the fact that step heat treated copper-containing-alloys generally resulted in an iron diffusion out of the 1:5 phase and that copper has a greater solubility in the 1:5 phase relative to the 2:17 phase (ref. 59) so that the 1:5 phase becomes magnetically softer. More recently, Krönmüller reported that on ageing, the 1:5 precipitates increase their domain wall energies, while the matrix has a decrease in domain wall energy (ref. 60).

ii) The Effect of Iron Additions on Magnetic Properties

It was shown by Strnat and Ray (ref. 54) that the substitution of Co by Fe in $RE_2(Co_{1-x}Fe_x)_{17}$ alloys induced easy c-axis behaviour in systems that had before exhibited only easy basal plane anisotropy and alloys with RE = Sm appeared to offer the best magnetic properties.

The room temperature values of induction ($4\pi M_s$) at 20 KOe along with the Curie temperature are shown in fig. 4.5 for varying iron contents. The increase in $4\pi M_s$ with increasing Fe content has been proposed to be caused by Fe atoms substitutionally replacing Co atoms (ref. 56) occupying sites around dumbbell pairs and so increasing the remanence, since the magnetic spin moment is greater in Fe than in Co and the anisotropy field is enhanced.

iii) The Effect on the Magnetic Properties of M Additions (M = Hf, Ti, Zr, Ni, Mn, Cr, Nb)

$Sm_2(Co,Cu,Fe)_{17}$ quarternary permanent magnetic alloys with the composition: Co, 26-27 wt.% Sm, 10-12 wt.% Cu and up to 8 wt.% Fe, were shown to yield energy products of up to 26 MGOe (ref. 61). In these alloys, a decrease of Cu content and/or an increase of Fe content induced a reduction of the coercive force. Therefore to develop a material with high $BH_{max}$, the effects of various other elemental additions were investigated. Ojima (ref. 62) found that additions of Zr to $Sm_2(Co,Cu,Fe)_{17}$ further improved the magnetic properties and in fact Zr was found to be the best additive; this will be discussed in the next section.

Satyanarayana et al (ref. 63) explored the effects on the primary magnetic properties of the elements Zr, V, Hf, Ti and Nb. It was found that the additions of these to a $Sm_2Co_{17-x}M_x$ alloy altered the crystal structure and increased the lattice parameter a, and decreased the c-axis length. It was suggested that these elements were substituting for cobalt in the $Sm_2Co_{17}$ lattice. This was indicated by a fall in the Curie temperature due to a weakening of the magnetic interaction. These results are shown in figs. 4.6 and 4.7.

iv) The Effect of Zirconium Additions on the Magnetic Properties

Zirconium has been found to produce the best magnetic properties in a $Sm_2(Co,Cu,Fe,M)_{17}$ system. It has been suggested that Zr increases the remanence by enhancing the dissolution of Fe in the 2:17 phase, thus increasing the uniaxial anisotropy, and Zr increases the

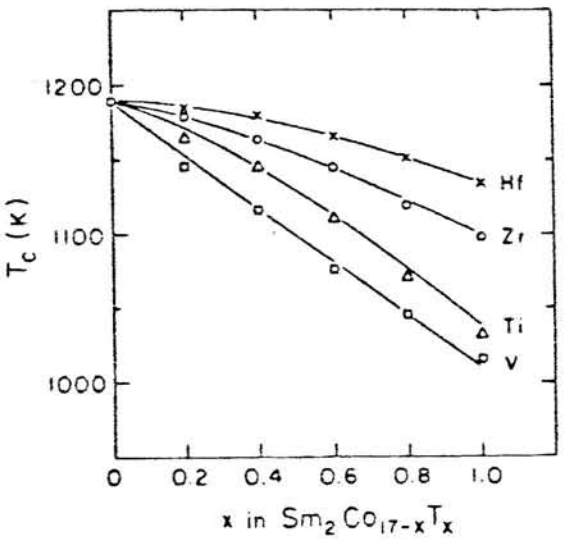


Fig. 4.6 Variation of the Curie Temperature ($T_c$) with composition in $Sm_2Co_{17-x}T_x$

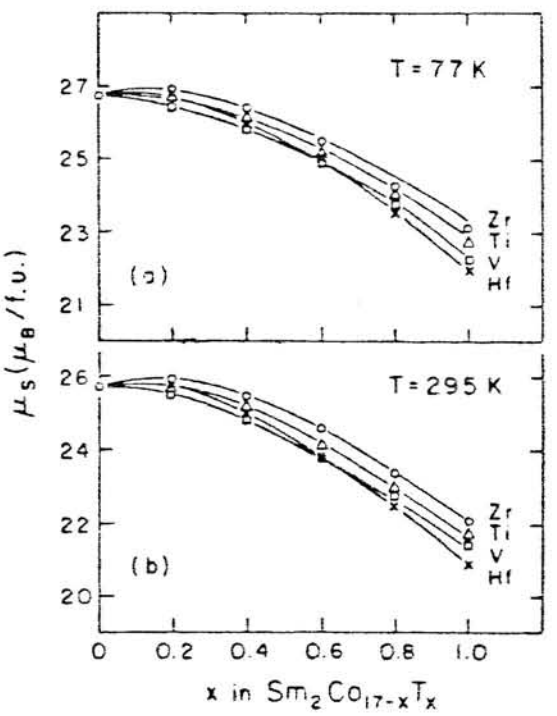


Fig. 4.7 Variation of saturation magnetic moment as a function of composition in $Sm_2Co_{17-x}T_x$.

coercivity by preferentially substituting in the 1:5 precipitates by replacing Sm and increasing the difference between the magneto-crystalline anisotropies of the 1:5 and 2:17 phases thus causing a more effective pinning of domain walls (ref. 56). Hadjipanayis (ref. 64) has shown that the presence of Zr controls the precipitate size and distribution. It was also shown that the Zr suppresses the formation of a SmCoCu phase which would lower the coercivity.

Yoneyma et al (ref. 65) looked at the effects of different Zr contents and found that the coercivity reaches a maximum value at different ageing times as the Zr content is varied this has also been observed in the present investigation (ref. 66) and by Kianvash and Harris (ref. 67). Yoneyma et al (ref. 65) proposed that this effect was due to the increased effectiveness of the 1:5 phase as a barrier to domain wall motion, and the 1:5 precipitates were reported as being thicker in the 3 wt.% Zr containing alloy.

v) The Effect of Microstructure on the Magnetic Properties

Transmission electron microscope (TEM) studies (refs. 31,68) of magnets of the type $Sm_2(Co,Cu,Fe,Zr)_{17}$ have revealed a cellular microstructure with 2:17 rhombohedral cells ($Th_2Zn_{17}$-type) surrounded by a fully coherent 1:5 hexagonal ($CaCu_5$-type) phase. The dimensions of the cells were found to be of the order of 300-500 Å in diameter and the cell walls about 40 Å thick.

It has also been reported that (refs. 64,69) superimposed on the cellular microstructure are elongated thin platelets or lamellae with a 1:3 type structure. Upon prolonged ageing Zr preferentially goes into the 1:3 phase; Cu goes into the 1:5

and 1:3 phases and Fe to the 2:17 phase.

During ageing Rabenburg (ref. 69) has shown that Zr plays a key role in aiding chemical partitioning between the 1:5 and 2:17 phases. He reported that the Zr is contained mainly in the 1:3 platelets which lie on the basal plane of the matrix phase, he designated this Zr-enriched phase the "Z-phase"; the number of Z-phase platelets being higher for the higher Zr content of 3 wt.%. The higher Zr content materials have been reported (ref. 69) to have a larger volume fraction of the 1:5 phase. Kianvash and Harris (ref. 70) have also reported the existence of a Zr rich phase which is depleted in Sm; optical microscopy showed the existence of a 1:5 cellular precipitate structure; the cells being about $10^4$ Å in diameter. These large 1:5 precipitates were assumed not to contribute to the coercivity, and domain pinning was ascribed to sub-optical precipitates.

According to Rabenburg (ref. 69), Zr tends to inhibit Sm diffusion at high temperatures; this is indicated by the differences in size of the microstructures for the 1.5 wt.% and 3 wt.% Zr alloys after similar heat treatments. The step ageing treatments are also more effective when there are significant Z phase plates in the matrix, the number of which is affected by the presence of Zr. Finally, Zr reduces the limits of solubility of Fe in the 1:5 phase and Cu in the 2:17 phase leading to greater compositional differences, thus producing more effective pinning sites.

The crystal structure morphology of the 2:17 type precipitation hardened magnets is shown in fig. 4.8 (ref. 71), where the Z phase

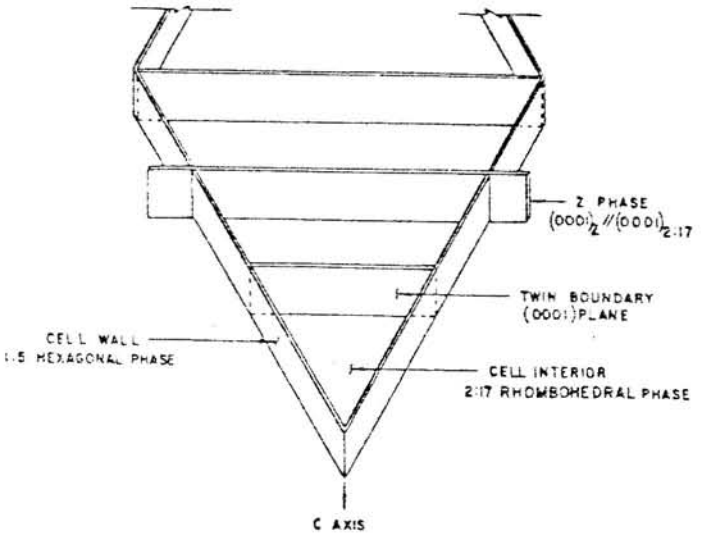


Fig. 4.8 Crystal morphology of "2:17"-type alloys.

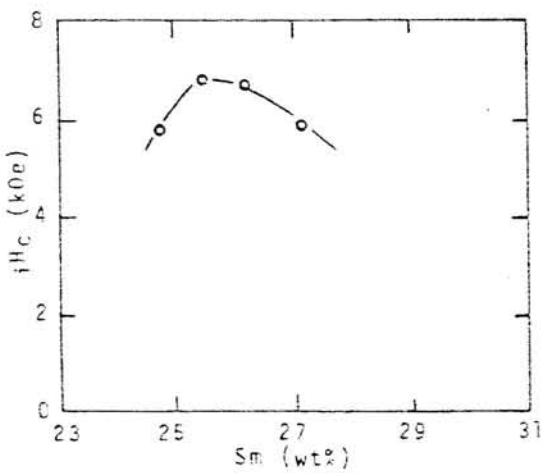


Fig. 4.9 $_{i}H_{c}$ versus wt.% Sm additions to a $Sm_2(Co,Cu,Fe,Zr)_{17}$-type alloy.

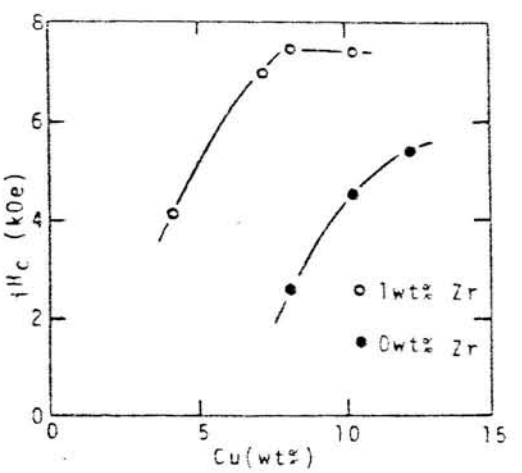


Fig. 4.10 $_{i}H_{c}$ versus wt.% Cu additions to a $Sm_2(Co,Cu,Fe,Zr)_{17}$-type alloy.

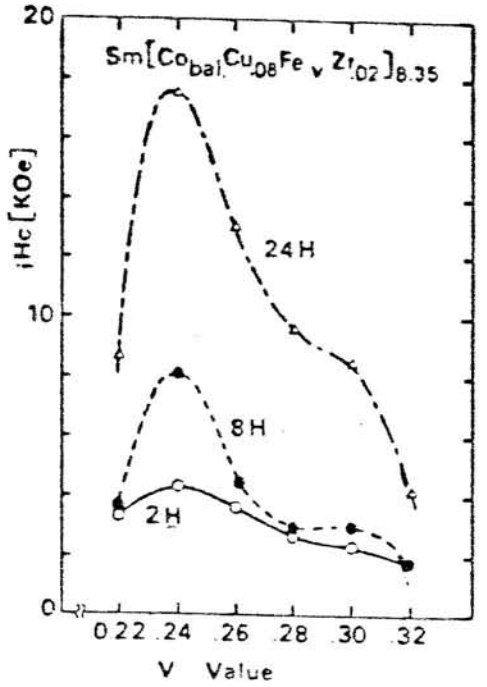


Fig. 4.11 $_{i}H_{c}$ versus Fe additions for a $Sm_2(Co,Cu,Fe,Zr)_{17}$-type alloy aged at different times at 800°C.

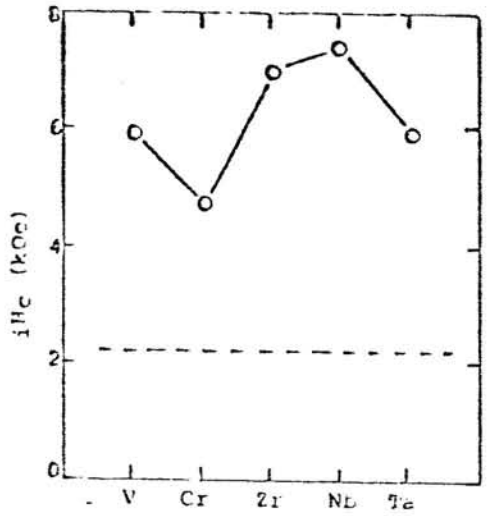


Fig. 4.12 Effects of V, Cr, Zr, Nb and Ta additions on $_{i}H_{c}$ for a $Sm_2(Co,Cu,Fe,Zr)_{17}$-type alloy.

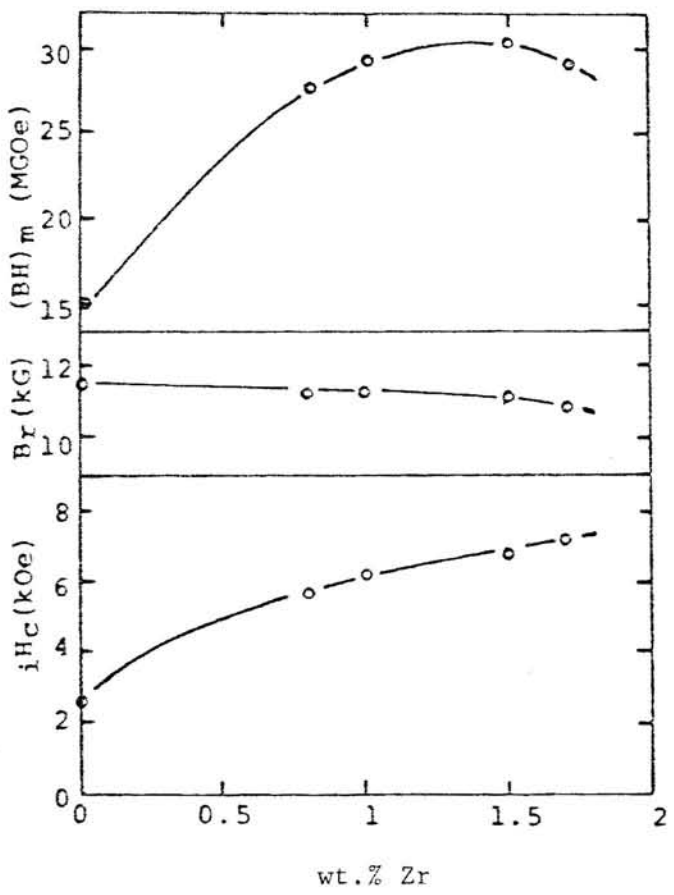


Fig. 4.13 Magnetic properties versus wt.% Zr additions on a $Sm_2(Co,Cu,Fe,Zr)_{17}$-type alloy.

is the 1:3 phase, and the effects of the various alloying additions are summarised in figs. 4.9 to 4.13.

### 4.3.3 Factors in Domain Pinning

The two phase magnetic alloys, such as those with the general composition: $Sm(Co,Cu,Fe,Zr)_z$ (z = 6 to 8.5) have coercivities generally governed by the effects of domain wall interactions with coherent precipitates.

Melton and Nagel (ref. 59) have studied a Sm-Co-Cu based material and discussed the factors affecting the pinning of domain walls. This alloy was found to consist of 1:5 type precipitates in a 2:17 type matrix. They suggested that since the magneto-crystalline energy was higher in the 1:5 precipitates observed, then the domain walls were obstructed upon moving into the precipitates. It has been proposed that the 1:5 type precipitates occurring in the $Sm(Co,Cu,Fe,Zr)_z$ alloy have "diluted" magnetic properties (that is, a lower magnetocrystalline anisotropy) due to a higher copper content than the matrix (refs. 64, 72); the domain walls are thus prevented from moving out of the precipitates.

Alloy additions ultimately affect the anisotropy and domain wall energy differences (ref. 53) between the two phases, and thus the extent of domain wall pinning, altering the coercivity of the material.

## 4.4 The Production of 2:17 Type Magnets

### 4.4.1 Resin Bonded Magnets

The two stages used by Shimoda et al (ref. 73) are shown in

fig. 4.14. The resin and powder mixture are cured in an applied magnetic field so that the particles align their c-axes with the field direction. The reason for using a lubricating binder in production method 2 was to attain better particle alignment, and so increase the remanence values.

The advantage of this process is that it is cheap and the materials can be machined fairly easily to the desired shape and size. However the densities attained are limited by the presence of the organic binder which decreases the remanence values.

### 4.4.2 Sintered Magnets

The basic processing involved to produce a sintered magnet may be outlined as below (ref. 62):

i) powder production

ii) aligning and pressing the powder in a magnetic field to produce a "green compact"

iii) sintering and solid solution treating (SST) the compact

iv) quenching to room temperature

v) ageing treatment to develop the magnetic properties.

The heat treatment stages are shown in fig. 4.15.

The advantages of sintering are that higher densities can be attained, so improving the remanence. The drawbacks are that high energy costs are involved and the material may be brittle and thus difficult to machine.

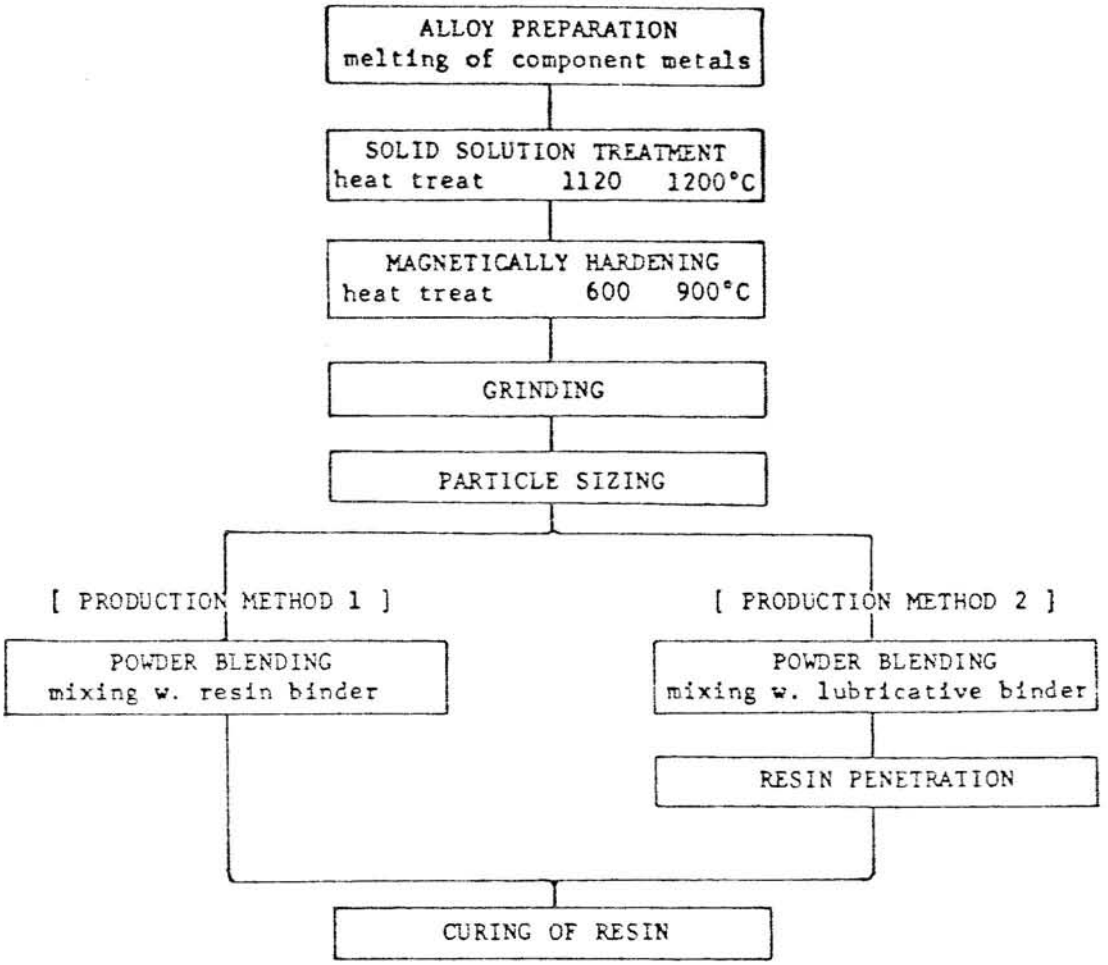


Fig. 4.14 Production steps used in producing resin-bonded "2:17"-type magnets.

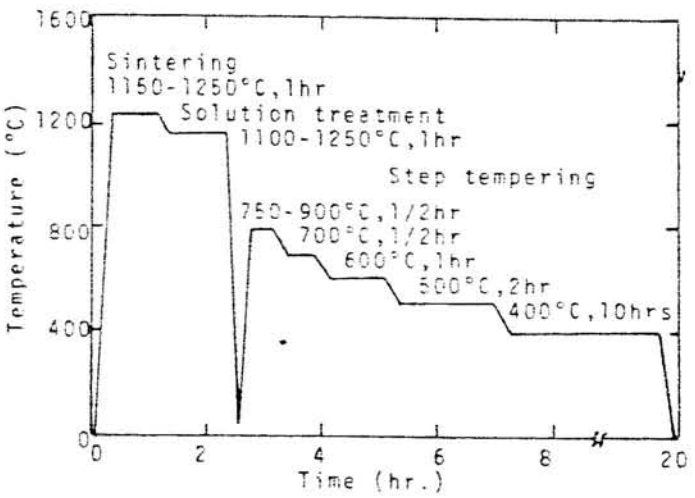


Fig. 4.15 Schematic of heat treatments used in producing "2:17"-type permanent magnets.

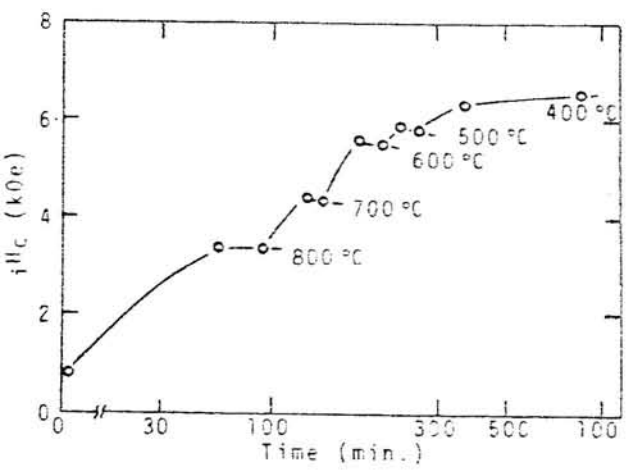


Fig. 4.16 Effect of step ageing on a "2:17"-type alloy.

A development of the sintering process is liquid phase sintering (LPS). The method involves using a lower melting point additive such as 60 wt.% Sm and 40 wt.% Co (ref. 74). In the case of $SmCo_5$ magnets it has been suggested that LPS gives higher densities (ref. 75), and a more homogeneous cellular structure, increasing the coercivity (ref. 76) as suggested by Livingston.

### 4.4.3 Effects of Heat Treatment on the Magnetic Properties

The production of both sintered and resin bonded magnets involves a solid solution heat treatment followed by an ageing treatment. According to Kianvash and Harris (ref. 70), for the optimum magnetic properties the SST should attain a homogeneous, almost single phase structure which is retained on quenching to room temperature. On ageing, the 1:5 type phase precipitates out as a fine cellular structure which acts to pin domains.

Sun (ref. 77) has reported that step ageing improves the coercivity to a greater extent in zirconium containing alloys than isothermal ageing. This was attributed to the fact that diffusion processes take place at high and low ageing temperatures: at the lower ageing temperatures copper diffuses out into the 1:5 phase, thus increasing the pinning effect. The Zr mainly enters this Cu rich 1:5 phase, further increasing the difference between the magnetocrystalline anisotropies of the 1:5 and 2:17 phases. Typical results for the effects of the ageing treatments on the coercivity are shown in fig. 4.16.

Rothwarf et al (ref. 78) have shown by TEM studies, that the 1:5 precipitate cell size decreases with decreasing ageing

temperature and along with accompanying shape changes, determines the coercivity.

Shimoda (ref. 73) found that the optimum coercivity solid solution temperature was around 1170$^{o}$C for a Z value of 8.35. Hadjipanayis (ref. 64) found the optimum temperature to be about 1185$^{o}$C but for a different composition. Kianvash (ref. 70) has proposed that at temperatures above the optimum solid solution temperature, melting occurs at grain boundaries or particle surfaces so an inhomogeneous microstructure results. Conversely at too low temperatures, inhomogeneity occurs due to a lack of diffusion of the component elements. These materials need to be manufactured under strict heat treatment schedules and compositional controls.